

# Energy conditions in static, spherically symmetric spacetimes and effective geometries

---

Zi-Liang Wang  <sup>a</sup> Emmanuele Battista  <sup>b</sup>

<sup>a</sup>*Department of Physics, School of Science, Jiangsu University of Science and Technology, Zhenjiang, 212003, China*

<sup>b</sup>*Istituto Nazionale di Fisica Nucleare, Laboratori Nazionali di Frascati, 00044 Frascati, Italy*

*E-mail:* [ziliang.wang@just.edu.cn](mailto:ziliang.wang@just.edu.cn),

[ebattista@lnf.infn.it](mailto:ebattista@lnf.infn.it), [emmanuelebattista@gmail.com](mailto:emmanuelebattista@gmail.com)

**ABSTRACT:** Classical energy conditions are investigated in generic static and spherically symmetric spacetimes. In setups with nonconstant  $g_{tt}g_{rr}$ , the appearance of horizons can signal the violation of the null energy condition and the breakdown of some standard near-horizon properties. For configurations satisfying  $g_{tt}g_{rr} = -1$ , we devise a systematic algorithm to generate solutions of the Einstein field equations that automatically obey the null energy condition. Within this family, we select a particularly significant metric that incorporates a logarithmic correction to the Schwarzschild model and fulfills all standard energy criteria. We examine its main features, including the horizon structure, geodesic behavior, and junction conditions. Our analysis shows that this geometry can be interpreted as an effective exterior description for both horizon-bearing and horizonless compact objects, and suggests that it can potentially act, in certain regimes, as a black hole mimicker.

**KEYWORDS:** Energy conditions; Effective geometries; Photon spheres; Innermost stable circular orbits; Compact objects; Black hole mimickers; Junction conditions.

---

## Contents

<b>1</b>	<b>Introduction</b>	<b>1</b>
<b>2</b>	<b>Static and spherically symmetric geometries</b>	<b>3</b>
2.1	Metrics with nonconstant $AB$	6
2.1.1	Case with $AB$ vanishing at some radius	6
2.1.2	Case with $AB$ different from zero	9
2.2	Solutions with $A(r) = 1/B(r)$	10
2.2.1	Constraints from NEC	11
2.2.2	Constraints from WEC	14
2.2.3	Constraints from SEC	15
2.2.4	Constraints from DEC	16
<b>3</b>	<b>Logarithmically corrected spacetime</b>	<b>16</b>
3.1	The $r = 0$ singularity	18
3.2	Horizon structure	18
3.3	Photon spheres and innermost stable circular orbits	20
3.4	Classification of horizon-bearing and horizonless configurations	22
3.5	Constraints from solar-system-like environments	27
3.5.1	Gravitational redshift	27
3.5.2	Bending of light	28
3.5.3	Orbit precession	29
3.6	Junction conditions	31
<b>4</b>	<b>Concluding remarks</b>	<b>33</b>
<b>A</b>	<b>Null energy condition in non-static and spherically symmetric geometries</b>	<b>34</b>

---

## 1 Introduction

Einstein equations relate spacetime curvature to the matter content, but if no suitable restrictions are imposed on the energy-momentum tensor  $T_{\mu\nu}$ , then, in principle, solutions can be generated *ad libitum* and geometries lacking any physical foundation are likely to be encountered. This undesirable situation can be avoided by enforcing classical energy conditions [1–8], which consist of pointwise inequalities requiring that various linear combinations of the components of  $T_{\mu\nu}$  take non-negative values. In this way, the notion that “normal” matter behaves in a physically reasonable way, i.e., consistently with classical expectations and such that gravity remains attractive, is implemented.

The weakest constraint on  $T_{\mu\nu}$  is the so-called null energy condition (NEC), which asserts that, for any null four-vector  $k^\mu$ , the following inequality must hold:

$$T_{\mu\nu}k^\mu k^\nu \geq 0, \quad (1.1)$$

while the weak energy condition (WEC) is expressed as

$$T_{\mu\nu}v^\mu v^\nu \geq 0, \quad (1.2)$$

with  $v^\mu$  any future-directed, normalized, timelike four-vector. The WEC implies the NEC by continuity and demands that the energy density locally measured by an observer with four-velocity  $v^\mu$  be non-negative, a property typically regarded as characteristic of “ordinary” (i.e., “non-exotic”) classical matter [9].

The assumption that gravity be always attractive in general relativity can be formulated via the strong energy condition (SEC) [5], which entails that

$$\left(T_{\mu\nu} - \frac{1}{2}T g_{\mu\nu}\right)v^\mu v^\nu \geq 0, \quad (1.3)$$

and clearly guarantees the NEC, but not necessarily the WEC, and is related to the so-called timelike convergence condition (see e.g. Ref. [10]).

Finally, the dominant energy condition (DEC) stipulates that no experimenter detects a negative energy density and that the associated energy-momentum flux  $J^\mu = -T^\mu{}_\nu v^\nu$  be future-directed and non-spacelike, ensuring that energy never propagates superluminally. These prescriptions amount to

$$T_{\mu\nu}v^\mu v^\nu \geq 0, \quad J^\mu J_\mu \leq 0, \quad (1.4)$$

and one can immediately see that DEC yields the WEC and hence the NEC.

Several foundational classical results rely on the validity of the above energy criteria, including the singularity [11–13], positive mass [14–16], and censorship [17, 18] theorems, as well as black hole thermodynamics [19, 20] and certain types of no-hair theorems [21, 22] (see e.g. Ref. [6] for further details). On the other hand, they are not fulfilled by many quantum fields (most famously in the Casimir effect and Hawking evaporation [3]), and even by some simple classical systems (in particular, the non-minimally coupled scalar fields [9], while minimally coupled massive scalar fields fail to obey the SEC [3]); a detailed list of classical and quantum violations can be found in Refs. [6, 7]. In response to these challenges, weaker statements are introduced: quantum energy inequalities provide (state-independent) lower bounds on weighted averages of  $\langle T_{\mu\nu} \rangle_{\text{ren}}$ , while the averaged energy conditions involve integrals of  $T_{\mu\nu}$  along suitable causal curves. The latter are weaker than the ordinary pointwise constraints and thus take an intermediate position between the classical criteria and the quantum ones [3, 5, 7, 23, 24].

One of the most significant settings restricted by standard energy conditions concerns the so-called exotic spacetimes [7], with traversable wormholes providing a prominent ex-

ample [3, 25]. Wormholes belong to the broad class of exotic compact objects and provide an example of black hole mimickers [26–34]. Such configurations are theoretically predicted in various extended theories of gravity, but also arise in certain general-relativistic scenarios (such as patterns involving beyond-the-standard-model fields minimally coupled to gravity, or exotic states of matter), and include fuzzballs [35, 36], gravastars [37–39], boson stars [40, 41], and several other proposals (see Table 1 in Ref. [28] for a complete taxonomy of exotic compact objects).

Reflecting the *classical* viewpoint that spacetimes failing to comply with energy conditions are often regarded as problematic, numerous models have been developed in which the necessary exotic matter can be minimized in suitable regimes. This occurs, for example, in some wormhole and gravastar configurations (see e.g. Refs. [42–49]), as well as for regularized black hole constructions known as “black-bounce” spacetimes [50, 51].

Motivated by this situation, in this paper we study classical energy conditions in static and spherically symmetric geometries within general relativity. We show that, in scenarios with nonconstant  $g_{tt}g_{rr}$ , horizons characterized by  $g_{tt}g_{rr} = 0$  can be associated with NEC violations. Moreover, in frameworks with  $-g_{tt} = g_{rr}^{-1}$ , we propose a systematic algorithm to construct metrics that adhere to the NEC. This procedure allows us to single out a particularly interesting case involving a logarithmic modification of the Schwarzschild model. This solution satisfies all energy conditions and can constitute an effective *geometric* candidate for describing the exterior spacetime of compact bodies, whether or not they carry an event horizon.

The structure of the paper is as follows. Classical energy criteria are analyzed in Sec. 2. The logarithmically corrected spacetime is thoroughly examined in Sec. 3, and concluding remarks are given in Sec. 4. Supplementary material is provided in the appendix.

*Conventions.* We use  $G = c = 1$  units, and metric signature  $(- + ++)$ .

## 2 Static and spherically symmetric geometries

In this section, we perform a detailed examination of classical energy conditions in the most general static and spherically symmetric spacetime

$$ds^2 = g_{\mu\nu}dx^\mu dx^\nu = -B(r)dt^2 + A(r)dr^2 + r^2d\Omega^2, \quad (2.1)$$

with  $d\Omega^2 = d\theta^2 + \sin^2\theta d\phi^2$  the line element on the two-sphere.

Energy criteria are most conveniently discussed in the local proper reference frame  $(\hat{t}, \hat{r}, \hat{\theta}, \hat{\phi})$  of a static observer [4, 19]. For this reason, we introduce the non-coordinate orthonormal basis in the standard manner [52, 53]:

$$e_a = e_a^\mu (\partial/\partial x^\mu), \quad (2.2a)$$

with the dual basis fulfilling

$$e^a = e^a_\mu dx^\mu, \quad (2.2b)$$

where Latin indices  $a, b, \dots = \hat{0}, \hat{1}, \hat{2}, \hat{3}$  denote frame components, Greek indices correspond to coordinate components, and  $e_a^\mu$  represents the inverse of  $e^a_\mu$ . These objects, referred to as tetrads (or vielbeins), form a  $4 \times 4$  matrix with positive determinant and satisfy the orthonormality condition

$$g_{\mu\nu} e_a^\mu e_b^\nu = \eta_{ab}, \quad (2.3)$$

as well as the completeness relation

$$g_{\mu\nu} = e^a_\mu e^b_\nu \eta_{ab}, \quad (2.4)$$

where  $\eta_{ab} = \text{diag}(-1, 1, 1, 1)$  is the Minkowski metric.

To construct the static basis, we choose  $e_{\hat{0}}$  to coincide with the experimenter four-velocity (i.e.,  $e_{\hat{0}}$  points along the observer time direction). By considering the static and spherically symmetric geometry (2.1), this procedure yields the tetrad field

$$e^a_\mu = \begin{cases} \text{diag}(\sqrt{B}, \sqrt{A}, r, r \sin \theta), & (B > 0, A > 0), \\ \text{diag}(\sqrt{-B}, \sqrt{-A}, r, r \sin \theta), & (B < 0, A < 0), \end{cases} \quad (2.5)$$

where the signs of  $B$  and  $A$  ensure that the metric retains always the Lorentzian signature. Specifically, when both  $B$  and  $A$  become negative (as occurs for instance inside the horizon of the Schwarzschild black hole), the coordinate basis vector  $\partial/\partial r$  becomes timelike while  $\partial/\partial t$  spacelike, indicating that no observer can remain at rest in the  $(r, \theta, \phi)$  coordinates.

In the static frame, the experimenter measures matter properties and expresses the energy-momentum tensor in the following diagonal form:

$$T_{ab} = T_{\mu\nu} e_a^\mu e_b^\nu = \text{diag}(\rho, p_1, p_2, p_3), \quad (2.6)$$

where  $\rho$  denotes the total density of mass-energy,  $p_1$  the radial pressure, while  $p_2$  and  $p_3$  the tangential pressures [54, 55]. In this way, the standard energy conditions translate into the following algebraic inequalities [4]:

$$\text{NEC} \Leftrightarrow \rho + p_i \geq 0, \quad (2.7a)$$

$$\text{WEC} \Leftrightarrow \rho \geq 0, \rho + p_i \geq 0, \quad (2.7b)$$

$$\text{SEC} \Leftrightarrow \rho + \sum_i p_i \geq 0, \rho + p_i \geq 0, \quad (2.7c)$$

$$\text{DEC} \Leftrightarrow \rho \geq 0, \rho \geq |p_i|, \quad (2.7d)$$

for all  $i = 1, 2, 3$ .

In the case with  $B > 0$  and  $A > 0$ , Einstein field equations imply that the energy

density and principal pressures entering Eq. (2.6) are given by

$$\rho = \frac{1 - (r/A)'}{8\pi r^2}, \quad (2.8a)$$

$$p_1 = \frac{-f_0}{8\pi r^2}, \quad (2.8b)$$

$$p_2 = p_3 = \frac{f_1}{8\pi r^2}, \quad (2.8c)$$

while for  $B$  and  $A$  both negative, we find

$$\rho = \frac{f_0}{8\pi r^2}, \quad (2.9a)$$

$$p_1 = -\frac{1 - (r/A)'}{8\pi r^2}, \quad (2.9b)$$

$$p_2 = p_3 = \frac{f_1}{8\pi r^2}, \quad (2.9c)$$

where the prime stands for the derivative with respect to the radial coordinate  $r$  and

$$f_0(r) := 1 - \left( \frac{1}{A} + \frac{rB'}{AB} \right), \quad (2.10)$$

$$f_1(r) := -\frac{rf_0'}{2} - \frac{r^2B'}{4} \left( \frac{1}{AB} \right)'. \quad (2.11)$$

It follows from the above expressions that NEC (2.7a) demands, in particular,

$$\rho + p_1 \geq 0, \quad (2.12)$$

thereby yielding

$$\frac{(AB)'}{rA^2B} \geq 0, \quad \text{for } B > 0, A > 0, \quad (2.13a)$$

$$-\frac{(AB)'}{rA^2B} \geq 0, \quad \text{for } B < 0, A < 0, \quad (2.13b)$$

which, in turn, leads to <sup>1</sup>

$$(AB)' \geq 0. \quad (2.14)$$

This inequality provides a *necessary but not sufficient* condition for the NEC to hold, in the sense that if  $(AB)' < 0$  for some range of  $r$ , then NEC is violated throughout that region. Relation (2.14) constrains the function  $A(r)B(r)$  to be non-decreasing. Specifically, since  $AB$  is not necessarily continuous for  $r > 0$  (for example,  $A$  diverges at the horizon of the Schwarzschild geometry), this monotonicity is required in each separate domain of continuity.

Our subsequent investigation will distinguish two cases, depending on whether  $AB \neq \mathcal{C}$  (see Sec. 2.1) or  $AB = \mathcal{C}$  (see Sec. 2.2), where  $\mathcal{C}$  is a constant. The key point is that

---

<sup>1</sup>It is worth noticing that by requiring the WEC for a regular black hole, Dymnikova [56] obtained a result similar to Eqs. (2.13) and (2.14).

in the latter situation one can always choose  $A = 1/B$  by absorbing  $\mathcal{C}$  into the definition of the time coordinate. This class of solutions is particularly relevant, as metrics like the Schwarzschild and Reissner-Nordström fall into this category. Furthermore, we will be mainly interested in asymptotically flat spacetimes, where for large  $r$  the components  $A(r)$  and  $B(r)$  comply with

$$\lim_{r \rightarrow \infty} A = 1, \quad (2.15a)$$

$$\lim_{r \rightarrow \infty} B = 1, \quad (2.15b)$$

which also imply

$$\lim_{r \rightarrow \infty} AB = 1. \quad (2.15c)$$

These prescriptions thus require the metric to approach the Minkowski form and all curvature invariants to vanish at spatial infinity, but they do not ensure a leading  $1/r$  falloff. As a consequence, it is not guaranteed that the associated Misner-Sharp-Hernandez mass (and hence the ADM mass) attains a finite, nonzero value in the limit  $r \rightarrow \infty$  [19, 57]. We will return to this point in Sec. 3.6.

## 2.1 Metrics with nonconstant $AB$

In this section, we consider metrics with  $AB \neq \mathcal{C}$ , and we further divide our analysis into two scenarios:  $AB$  vanishes for some value of  $r$  (see Sec. 2.1.1);  $AB \neq 0 \forall r > 0$  (see Sec. 2.1.2).

### 2.1.1 Case with $AB$ vanishing at some radius

The relation  $AB = 0$  defines a hypersurface where the metric is degenerate, i.e.,  $\det g_{\mu\nu} = 0$ . In such circumstances, index raising becomes ambiguous and the Levi-Civita connection typically diverges (see Ref. [58] for details and e.g. Refs. [59–69] for some applications of degenerate metrics in cosmology and black hole models). In the following, we thus examine the limiting regime  $AB \rightarrow 0$ , while maintaining the validity of Einstein theory of gravity. Our aim is to identify nonstandard physical phenomena emerging in this critical setting, where conventional spacetime descriptions may require careful assessment.

The condition  $AB = 0$  at some radius may arise in two distinct ways <sup>2</sup>: (i)  $A = 0$ ; (ii)  $B = 0$ .

In the scenario (i), it is evident from Eqs. (2.8) and (2.9) that the energy density  $\rho$  blows up at points where  $A = 0$ . Although this pathological behavior could be avoided by assuming  $A \neq 0$ , we refrain from doing so in order to retain generality in the subsequent analysis.

The situation (ii) is more subtle, as the identity  $B = 0$  marks the location of the event horizon(s). In this case, the construction (2.5) breaks down because the static experimenter four-velocity becomes infinite, and hence the ensuing interpretation of the energy density

---

<sup>2</sup>We leave aside the case where both  $A$  and  $B$  vanish simultaneously, as it yields rather exotic situations; for instance, the energy density inevitably blows up in both the static basis and the freely falling frame, which we introduce below.

and pressures becomes ill-defined. This issue can be resolved by adopting the orthonormal frame, say  $\{e_{a'}{}^\mu\}$ , adapted to a freely falling radial observer with four-velocity  $v^\mu$ .

The timelike basis vector  $e_{\hat{0}'}{}^\mu$  is identified with  $v^\mu$ , which in the geometry (2.1) is given by

$$v^\mu = \frac{dx^\mu}{d\lambda} = \left( \frac{E}{B}, -\sqrt{\frac{1}{A} \left( \frac{E^2}{B} - 1 \right)}, 0, 0 \right), \quad (2.16)$$

where we have exploited the normalization condition  $v^\mu v_\mu = -1$ ,

$$E \equiv B(r) \frac{dt}{d\lambda}, \quad (2.17)$$

is the conserved energy per unit rest mass associated with the Killing vector field  $\partial_t$ , and  $\lambda$  represents the affine parameter. The tetrad can now be completed with the three mutually orthogonal spacelike unit vectors:

$$e_{\hat{1}'}{}^\mu = \left( -\frac{\sqrt{E^2 - B}}{B}, \frac{E}{\sqrt{AB}}, 0, 0 \right), \quad (2.18)$$

$$e_{\hat{2}'}{}^\mu = \left( 0, 0, \frac{1}{r}, 0 \right), \quad (2.19)$$

$$e_{\hat{3}'}{}^\mu = \left( 0, 0, 0, \frac{1}{r \sin \theta} \right), \quad (2.20)$$

where  $e_{\hat{1}'}{}^\mu$  is constructed to be orthogonal to  $e_{\hat{0}'}{}^\mu$  and normalized as  $g_{\mu\nu} e_{\hat{1}'}{}^\mu e_{\hat{1}'}{}^\nu = 1$ .

The freely falling basis allows for a physically meaningful interpretation of the energy-momentum tensor  $T_{a'b'} = T_{\mu\nu} e_{a'}{}^\mu e_{b'}{}^\nu$  at the event horizon. The nonvanishing components read as

$$T_{\hat{0}'\hat{0}'} \equiv \rho^{\text{ff}} = \frac{1}{8\pi r^2} \left[ f_0 - E^2 r \left( \frac{1}{AB} \right)' \right], \quad (2.21a)$$

$$T_{\hat{1}'\hat{1}'} \equiv p_1^{\text{ff}} = \frac{1}{8\pi r^2} \left[ -1 + \left( \frac{r}{A} \right)' - E^2 r \left( \frac{1}{AB} \right)' \right], \quad (2.21b)$$

$$T_{\hat{2}'\hat{2}'} \equiv p_2^{\text{ff}} = \frac{f_1}{8\pi r^2} = T_{\hat{3}'\hat{3}'} \equiv p_3^{\text{ff}}, \quad (2.21c)$$

$$T_{\hat{0}'\hat{1}'} = T_{\hat{1}'\hat{0}'} = \frac{E\sqrt{E^2 - B}}{8\pi r^2 B} \left[ f_0 - 1 + \left( \frac{r}{A} \right)' \right], \quad (2.21d)$$

where the off-diagonal term  $T_{\hat{0}'\hat{1}'}$ , which is absent in Eq. (2.6) and vanishes identically in the special case  $A = 1/B$ , quantifies the radial energy flux density in the experimenter local rest frame. Moreover, since the divergence stemming from the derivative of  $1/(AB)$  cannot, in general, be canceled for all possible values of the energy  $E$ , both  $\rho^{\text{ff}}$  and  $p_1^{\text{ff}}$  typically become unbounded as  $AB \rightarrow 0$ .

Interestingly, in the static tetrad (2.5) these divergences may be obscured by coordinate-dependent artifacts. This point can be illustrated by two explicit examples where we assume that the metric (2.1) can be expanded near a horizon located at  $r = r_h$  (defined by  $B(r_h) =$

0) with the following leading-order terms:

$$\text{Example 1:} \quad A(r) \sim (r - r_h)^{-2}, \quad B(r) \sim (r - r_h)^3, \quad (2.22)$$

$$\text{Example 2:} \quad A(r) \sim (r - r_h)^{-3}, \quad B(r) \sim (r - r_h)^5. \quad (2.23)$$

As one can easily verify from Eqs. (2.8) and (2.9), the energy density and principal pressures detected by the static observer remain finite as  $r \rightarrow r_h$ , while the corresponding quantities evaluated in the freely falling reference system blow up. Nevertheless, no curvature singularity is present at the horizon, since for both examples the Ricci scalar stays regular as  $r \rightarrow r_h$

$$\text{Example 1:} \quad R \sim \frac{-33r^2 + 28rr_h - 4r_h^2 + 4}{2r^2}, \quad (2.24)$$

$$\text{Example 2:} \quad R \sim \frac{-33r^3 + 53r^2r_h - 22rr_h^2 + 2r_h^3 + 2}{r^2}, \quad (2.25)$$

and the Kretschmann invariant  $\mathcal{K} = R_{\mu\nu\rho\sigma}R^{\mu\nu\rho\sigma}$  displays the same trend.

In addition, the above scenarios allow us to prove that when  $AB = 0$  the metric can admit two possible behaviors: either its signature shifts from Lorentzian to Euclidean across  $r = r_h$  (as in the first case (2.22)), or it remains Lorentzian throughout, but NEC is violated in the region  $r < r_h$  (as one can readily demonstrate in the second case (2.23)).

To further explore the physical implications of the condition  $AB = 0$ , we now consider the radial geodesic equation. In the spacetime (2.1), it is given by

$$\frac{1}{2} \left( \frac{dr}{d\lambda} \right)^2 - \frac{E^2}{2AB} + \frac{\alpha}{2A} = 0, \quad (2.26)$$

which resembles the dynamics of a particle with unit effective mass and zero energy moving in the one-dimensional ‘‘radial’’ effective potential

$$\mathcal{V}_{\text{eff}}^r = -\frac{E^2}{2AB} + \frac{\alpha}{2A}, \quad (2.27)$$

with  $\alpha = 1, 0$  for timelike and null geodesics, respectively. As  $AB \rightarrow 0$ ,  $\mathcal{V}_{\text{eff}}^r$  tends to infinity, and we can conceive two situations:

- $AB \rightarrow 0^\pm$  when  $r \rightarrow r_h^\pm$ . Under these hypotheses, we have an infinite potential well at  $r_h^+$  and an infinite potential barrier at  $r_h^-$ . In the outer domain  $r > r_h$ , particles are attracted toward the horizon but cannot cross it, while in the inner region a turning point develops before the horizon is reached.
- $AB \rightarrow 0^+$  for  $r \rightarrow r_h^\pm$ . In this case, an infinite potential well forms on both sides of  $r = r_h$ .

In both scenarios, the horizon thus acts effectively as a two-way impenetrable surface, which cannot be traversed from either direction.

This ‘‘impenetrable boundary’’ conclusion is reinforced by the expansion scalar  $\vartheta$  of the congruence of ingoing radial geodesics, which in any static, spherically symmetric spacetime

(2.1) satisfies the geometric identity [4, 70]

$$\vartheta = \frac{\alpha(rB' + 4B) - 4E^2}{2r\sqrt{AB}\sqrt{E^2 - \alpha B}}. \quad (2.28)$$

Both for the null and timelike cases,  $\vartheta \rightarrow -\infty$  as  $AB \rightarrow 0^+$  and  $E$  takes sufficiently large values. This divergence signals the occurrence of a caustic and may indicate the presence of conjugate points along the congruence<sup>3</sup>, a standard indicator of geodesic incompleteness [19]. Interestingly, for timelike (i.e.,  $\alpha = 1$ ) infalling radial paths,  $\vartheta$  can become positive when  $rB' > 4(E^2 - B)$ , and energy conditions may be violated. We will discuss this situation in detail in Sec. 2.2.2.

From the above analysis, it is clear that when the metric retains the Lorentzian signature, the fulfillment of the NEC implies that a singularity may arise at points where  $AB \rightarrow 0^+$ , even though curvature may not attain unboundedly large values. This outcome is fully consistent with the expectations of classical singularity theorems [13]. Although our examination is primarily based on general relativity and focuses on the region  $r > 0$  of the spacetime, the result that  $AB \rightarrow 0$  implies a potential singularity can be straightforwardly generalized to the case  $r = 0$  or to other modified theories of gravity admitting static, spherically symmetric metrics. This conclusion is supported by several models with  $A \neq 1/B$ , such as the Janis-Newman-Winicour spacetime [71–73] and certain Brans-Dicke solutions [74, 75], in which naked singularities appear at  $r = 0$  accompanied by the vanishing of the product  $AB$ .

The examination of this section can be relevant for numerous effective or quantum-inspired black holes, in which the underlying corrections lead to scenarios where  $A(r)$  remains finite as  $B(r) \rightarrow 0$  (see e.g. Refs. [76–80]), so that the product  $AB \rightarrow 0$  at the horizon. As we have shown before, in this setup new effects departing from the classical Schwarzschild paradigm can arise. Such phenomena may indicate a breakdown of the equivalence principle at the horizon and suggest the presence of novel near-horizon physics beyond the classical pattern [81].

Similar effects as those encountered in this section can emerge in non-static and spherically symmetric geometries, for which we investigate the NEC in Appendix A.

### 2.1.2 Case with $AB$ different from zero

According to the discussion of the previous section, the requirement  $AB \neq 0$  serves to prevent several undesired features, including NEC violations and metric-signature changes. For this reason, we now assume that  $AB \neq 0$  throughout the spacetime except at  $r = 0$ , where a curvature singularity may exist.

---

<sup>3</sup>In general, the existence of conjugate points signals the presence of extrema-length curves. Consider a spacelike hypersurface  $\Sigma$  and a timelike geodesic congruence orthogonal to  $\Sigma$ ; a point  $p$  on one geodesic of the congruence is said to be conjugate to  $\Sigma$  if and only if the expansion scalar  $\vartheta$  tends to  $-\infty$  at  $p$ . For instance, in Schwarzschild spacetime, conjugate points appear along ingoing radial timelike geodesics as  $\vartheta \rightarrow -\infty$  when  $r \rightarrow 0$ . This behavior implies that the proper lengths of these geodesics are bounded from above in the future direction, indicating geodesic incompleteness.

The necessary condition (2.14) for the NEC fulfillment implies that, under the hypothesis that  $AB$  is a smooth function,  $(AB)'$  can only be zero at isolated points. Therefore,  $AB$  is monotonically increasing in its domains except where  $(AB)' = 0$ . Since, in an asymptotically flat spacetime, the metric functions  $A(r)$  and  $B(r)$  comply with Eq. (2.15), the quantity  $AB$  is restricted to values not exceeding 1. These considerations lead to the following conclusion:

In the asymptotically flat, static, and spherically symmetric spacetime (2.1), the smooth function  $AB$  must satisfy one of the following conditions, otherwise either NEC is violated or the metric signature changes from Lorentzian to Euclidean—both of which can potentially lead to geodesic incompleteness:

- (i)  $AB$  is constant for all  $r > 0$ ,
- (ii)  $0 < AB \leq 1$  for all  $r > 0$ .

In this situation, the metric can be expressed as

$$ds^2 = -B(r)dt^2 + \frac{F(r)}{B(r)}dr^2 + r^2d\Omega^2, \quad (2.29)$$

with

$$0 < F(r) \leq 1. \quad (2.30)$$

Notice that, for a black hole solution, the above statement entails that a constant- $r$  null hypersurface must also be a metric horizon. Indeed, the latter is identified by the equation  $B(r_h) = 0$ , and hence the constraint that  $AB$  remains finite yields  $A \rightarrow \infty$  at  $r = r_h$ .

## 2.2 Solutions with $A(r) = 1/B(r)$

We now turn to the case  $AB = \mathcal{C}$ , where the constant  $\mathcal{C}$  is nonzero in order to avoid a trivial, nonphysical solution.

As pointed out before, in this setup it is always possible to set  $A = 1/B$  and then express the metric as

$$ds^2 = -B(r)dt^2 + \frac{dr^2}{B(r)} + r^2d\Omega^2. \quad (2.31)$$

This spacetime belongs to the so-called Kerr-Schild class (see e.g. Refs. [30, 82, 83]). We now examine the constraints imposed by the NEC (Sec. 2.2.1), WEC (Sec. 2.2.2), SEC (Sec. 2.2.3), and DEC (Sec. 2.2.4). As we will see, our investigation allows us to devise an algorithm for generating solutions to Einstein field equations of the form (2.31) that automatically comply with NEC (see Eqs. (2.33) and (2.34) below).

### 2.2.1 Constraints from NEC

By adopting the static tetrad (cf. Eq. (2.5)), we find from Eq. (2.8) that the energy density and principal pressures for the spacetime (2.31) take the form

$$\rho = \frac{1 - B - rB'}{8\pi r^2}, \quad (2.32a)$$

$$p_1 = -\rho, \quad (2.32b)$$

$$p_2 = p_3 = \frac{rB'' + 2B'}{16\pi r}. \quad (2.32c)$$

This means that the NEC (2.7a) is satisfied if and only if

$$y(r) \geq 0, \quad (2.33)$$

where we have introduced the  $r$ -dependent function

$$y(r) = r^2 B''(r) - 2B(r) + 2. \quad (2.34)$$

To explore some explicit examples meeting the constraint (2.33), we consider the *ansatz*

$$y(r) = c_n r^n, \quad (2.35)$$

where  $c_n \geq 0$  are constants and  $n$  is an integer (this choice is made for simplicity, as our results extend straightforwardly also to non-integer values of  $n$ ). In this way, Eq. (2.34) can be read as an ordinary differential equation whose solutions produce metric functions  $B(r)$  that automatically obey the NEC. Let us consider the following choices for  $y(r)$ :

- $y(r) = 0$ . In this case, Eq. (2.34) becomes a homogeneous differential equation and we readily obtain

$$B(r) = 1 - \frac{d_1}{r} - d_2 r^2, \quad (2.36)$$

with  $d_{1,2}$  (dimensionful) integration constants. Within our class of solutions, Eq. (2.36) is the only one that gives rise to an isotropic energy-momentum tensor, whereas the other configurations necessarily involve anisotropic pressures (cf. Eq. (2.32)). Setting  $d_1 = R_S \equiv 2M$  and  $d_2 > 0$ , we obtain the Schwarzschild-de Sitter metric. Thus, to maintain consistency with this physical interpretation, we will henceforth fix  $d_1 = R_S \equiv 2M$  (more details on the parameter  $M$  will be given in Sec. 3.6).

- $y(r) = c_0$ . For this scenario, Eq. (2.34) yields the solution

$$B(r) = 1 - \frac{R_S}{r} - d_2 r^2 - \frac{c_0}{2}. \quad (2.37)$$

- $y(r) = c_{-1}/r$ .

$$B(r) = 1 - \frac{R_S}{r} - d_2 r^2 - \frac{c_{-1} \ln r}{3r}. \quad (2.38)$$

- $y(r) = c_2 r^2$ .

$$B(r) = 1 - \frac{R_S}{r} - d_2 r^2 + \frac{c_2 r^2 \ln r}{3}. \quad (2.39)$$

- $y(r) = c_m r^m$  with  $m \neq 2$  and  $m \neq -1$ .

$$B(r) = 1 - \frac{R_S}{r} - d_2 r^2 + \frac{c_m r^m}{m^2 - m - 2}. \quad (2.40)$$

In this situation, we can recover the Reissner-Nordström metric by taking  $m = -2$  and  $d_2 = 0$ .

In the above discussion, we have neglected dimensions for simplicity. Since the function  $y(r)$  is dimensionless, it is convenient to take  $c_n$  to be dimensionless as well. To ensure this, a length scale  $r_d$  should be introduced into Eq. (2.35), which can be thus reexpressed as  $y(r) = c_n (r/r_d)^n$ . For instance, setting  $y = c_{-1} (r_d/r)$  Eq. (2.38) reads as (recall that  $d_2$  is dimensionful)

$$B(r) = 1 - \frac{R_S}{r} - d_2 r^2 - \frac{c_{-1} r_d \ln(r/r_d)}{3r}. \quad (2.41)$$

The parameter  $r_d$  could be identified with  $R_S$  or another relevant physical scale, such as the Planck length, depending on the context of the problem. In the remainder of this section, we will omit  $r_d$  for simplicity, but we will restore it in the examination of Sec. 3.

Since relation (2.34) gives rise to a linear differential equation, the superposition principle applies, guaranteeing that any linear combination of Eqs. (2.37)–(2.40) still solves Eq. (2.34). Consequently, if we write

$$y(r) = \sum_n c_n r^n, \quad (2.42)$$

then  $B(r)$  takes the general form

$$B(r) = 1 - \frac{R_S}{r} - d_2 r^2 - \frac{c_{-1} \ln r}{3r} + \frac{c_2 r^2 \ln r}{3} + \sum_{n \neq -1, 2} \frac{c_n r^n}{n^2 - n - 2}, \quad (2.43)$$

and condition (2.33) automatically holds as long as  $c_n \geq 0$  for all terms in the sum (2.42).

Since we have adopted an *ansatz* to enforce the requirement (2.33), there also exist NEC-satisfying configurations that are not captured by Eq. (2.43), such as the well-known regular black hole models (which, we recall, typically spoil the SEC) [84–86]. Nevertheless, our result (2.43) provides a straightforward criterion for assessing NEC violations in numerous modified Schwarzschild and quantum-corrected black hole geometries studied in the literature (see e.g. Refs. [76, 80, 87–89]). For example, if  $B(r)$  has the form

$$B(r) = 1 - \frac{R_S}{r} + \frac{c_i}{r^i}, \quad \text{with } i \geq 2, \quad (2.44)$$

NEC is respected if and only if  $c_i \geq 0$ , and similarly for

$$B(r) = 1 - \frac{R_S}{r} + \frac{c_i}{r^i} + \frac{c_m}{r^m}, \quad \text{with } 2 \leq i < m, \quad (2.45)$$

NEC is met if and only if  $c_i \geq 0$  and  $c_m \geq 0$ .

We emphasize that the lower bound  $c_n \geq 0$  for the coefficients in the sum (2.42) represents in general a sufficient, though not a necessary, condition for the NEC to hold (the cases (2.44) and (2.45) admit necessary *and* sufficient conditions because they contain few parameters). To illustrate this point, we now discuss a scenario where some  $c_n$  may be negative while the constraint (2.33), and hence the NEC, is fulfilled.

For physical relevance, we consider an asymptotically flat spacetime, with

$$B(r) = 1 - \frac{R_S}{r} + \frac{c_i}{r^i} + \frac{c_m}{r^m} + \frac{c_n}{r^n}, \quad \text{where } 2 \leq i < m < n. \quad (2.46)$$

The function  $y(r)$  defined in Eq. (2.34) then becomes

$$y(r) = \frac{c_i(i^2 + i - 2)}{r^i} + \frac{c_m(m^2 + m - 2)}{r^m} + \frac{c_n(n^2 + n - 2)}{r^n}, \quad (2.47)$$

and exhibits the asymptotic behavior

$$y(r) \rightarrow \begin{cases} \frac{c_i(i^2+i-2)}{r^i}, & \text{as } r \rightarrow \infty, \\ \frac{c_n(n^2+n-2)}{r^n}, & \text{as } r \rightarrow 0. \end{cases} \quad (2.48)$$

To secure condition (2.33) in the limits  $r \rightarrow 0$  and  $r \rightarrow \infty$ , it is necessary that  $c_n \geq 0$  and  $c_i \geq 0$ , while ensuring that  $y(r)$  remains non-negative throughout its domain further requires that

$$c_m(m^2 + m - 2) \geq -c_i(i^2 + i - 2)r^{m-i} - c_n(n^2 + n - 2)/r^{n-m}. \quad (2.49)$$

The maximization of the right-hand side of Eq. (2.49) is given by

$$\begin{aligned} -\mathcal{F} &= -c_i(i^2 + i - 2) \left[ \frac{c_n(n^2 + n - 2)(n - m)}{c_i(i^2 + i - 2)(m - i)} \right]^{\frac{m-i}{n-i}} \\ &- c_n(n^2 + n - 2) \left[ \frac{c_i(i^2 + i - 2)(m - i)}{c_n(n^2 + n - 2)(n - m)} \right]^{\frac{n-m}{n-i}}, \end{aligned} \quad (2.50)$$

which means that the necessary and sufficient condition to satisfy the NEC is

$$c_{i,n} \geq 0, \quad \text{and } c_m \geq -\frac{\mathcal{F}}{m^2 + m - 2}. \quad (2.51)$$

Since  $\mathcal{F}$  is positive, it follows that  $c_m$  can indeed be negative, as pointed out before.

From our analysis it is clear that Eqs. (2.33) and (2.34) provide a systematic method for producing metrics in the Kerr-Schild form (2.31) that adhere to the NEC, the only input

being an *ansatz* for the function  $y(r)$ , as done in Eqs. (2.35) and (2.42). A key advantage of this procedure is that it enables one to determine a broad family of geometries, including the well-known Schwarzschild, Schwarzschild-de Sitter, and Reissner-Nordström solutions. Table 1 summarizes the necessary *and* sufficient conditions for the NEC to apply for some of the ensuing configurations.

Metric function $B(r)$	Necessary and sufficient conditions for the NEC
$1 - \frac{R_S}{r} + \frac{c_i}{r^i}$	$c_i \geq 0$
$1 - \frac{R_S}{r} + \frac{c_i}{r^i} + \frac{c_m}{r^m}$	$c_i \geq 0, \quad c_m \geq 0$
$1 - \frac{R_S}{r} + \frac{c_i}{r^i} + \frac{c_m}{r^m} + \frac{c_n}{r^n}$	$c_i \geq 0, \quad c_n \geq 0, \quad c_m \geq -\mathcal{F}/(m^2 + m - 2)$

**Table 1:** Necessary and sufficient conditions for the NEC to be respected by static and spherically symmetric metrics of the Kerr-Schild form (2.31). For all the cases analyzed, it is understood that  $2 \leq i < m < n$ . The parameter  $\mathcal{F}$  can be read off from Eq. (2.50).

Since the NEC does not necessarily guarantee compliance with the WEC, SEC, and DEC, in the next sections we examine the restrictions due to these tighter conditions and show that they lead to additional limitations on the metric function (2.43).

### 2.2.2 Constraints from WEC

When we impose the validity of the WEC (2.7b), it follows from Eq. (2.32a) that, in addition to Eq. (2.33), the metric component  $B(r)$  is subject to the further constraint

$$1 - B - rB' \geq 0, \quad (2.52)$$

which, for the general solution (2.43), translates into

$$9d_2r^2 + \frac{c_{-1}}{r} - c_2r^2(1 + 3 \ln r) - 3 \sum_{n \neq -1, 2} \frac{c_n r^n}{n-2} \geq 0. \quad (2.53)$$

To assess whether the WEC holds, we analyze each term on the left-hand side separately. Taking  $d_2 \geq 0$  guarantees that the first contribution complies with the WEC, while the second does so automatically, since the NEC already enforces  $c_{-1} \geq 0$ . However, the third factor proportional to  $c_2$  can become negative, and hence satisfying the WEC necessitates setting  $c_2 = 0$ . Finally, for the remaining sum, a sufficient condition for non-negativity is  $n < 2$ , along with the bound  $c_n \geq 0$ , as already mandated by NEC.

We can now prove that if the expansion scalar  $\vartheta$ , computed in Eq. (2.28), becomes positive along ingoing radial timelike geodesics, then WEC is necessarily spoiled. To this end, we consider a massive particle initially at rest at some radius  $r$ , which then begins to

free-fall toward  $r = 0$ . This onset is triggered when

$$\frac{d}{dr} \mathcal{V}_{\text{eff}}^{r, \text{timelike}} > 0, \quad (2.54)$$

where the “timelike” effective potential  $\mathcal{V}_{\text{eff}}^{r, \text{timelike}}$  is obtained from Eq. (2.27) by substituting  $A = 1/B$  and  $\alpha = 1$ . The above inequality entails

$$B' > 0, \quad (2.55)$$

while the WEC imposes Eq. (2.52), which is equivalent to

$$rB' < 1 - B. \quad (2.56)$$

Taken together, the bounds (2.55) and (2.56) imply that  $1 - B > 0$ . Now, let us examine radially moving massive bodies released from rest in the asymptotically flat region  $r \rightarrow \infty$ , for which the conserved energy takes the value  $E = 1$ . In this situation, the condition  $\vartheta > 0$  yields

$$rB' > 4(1 - B), \quad (2.57)$$

which is clearly incompatible with Eq. (2.56) in the physically relevant domain  $B < 1$ . Consequently, within this setup, if the WEC holds the congruence must satisfy  $\vartheta \leq 0$ , corresponding to the non-expanding regime in which observers experience neither defocusing nor local repulsive effects.

### 2.2.3 Constraints from SEC

Starting from Eq. (2.32), one readily finds that the SEC (2.7c) is valid if and only if Eq. (2.33) is supplemented by

$$B'' + \frac{2B'}{r} \geq 0, \quad (2.58)$$

which, when applied to the metric coefficient (2.43), reduces to

$$-6d_2 + \frac{c_{-1}}{3r^3} + c_2(2 \ln r + 5/3) + \sum_{n \neq -1, 2} \frac{nc_n r^{n-2}}{n-2} \geq 0. \quad (2.59)$$

If  $d_2 > 0$ , the first term on the left-hand side circumvents SEC, a result fully consistent with the interpretation of  $d_2 > 0$  as corresponding to a positive cosmological constant. The second factor complies with the SEC as  $c_{-1} \geq 0$  owing to NEC, while for  $c_2 > 0$  the third one violates the SEC, since it can become negative for sufficiently small  $r$ . A sufficient condition for the last contribution involving the sum to remain non-negative is  $n \leq 0 \cup n > 2$  jointly with  $c_n \geq 0$ .

### 2.2.4 Constraints from DEC

The DEC (2.7d) demands that Eq. (2.33) be combined with Eq. (2.52) and

$$r^2 B''(r) + 4rB'(r) + 2B(r) - 2 \leq 0, \quad (2.60)$$

which gives

$$12d_2 r^2 + \frac{c_{-1}}{3r} - c_2 r^2 \left( \frac{7}{3} + 4 \ln r \right) - \sum_{n \neq -1, 2} \frac{c_n (n+2) r^n}{n-2} \geq 0. \quad (2.61)$$

This inequality holds for all  $r > 0$  if  $d_2 \geq 0$ ,  $c_{-1} \geq 0$ , and  $c_2 = 0$ , which are already demanded by the WEC. Moreover, a sufficient condition for the sum to be non-negative is  $-2 \leq n < 2$ , which is stronger than the requirement imposed by the WEC.

<b>Metric function:</b> $B(r) = 1 - \frac{R_S}{r} - d_2 r^2 - \frac{c_{-1} \ln r}{3r} + \frac{c_2 r^2 \ln r}{3} + \sum_{n \neq -1, 2} \frac{c_n r^n}{n^2 - n - 2}$	
<b>Energy condition</b>	<b>Sufficient conditions on the coefficients of <math>B(r)</math></b>
NEC	$c_{-1} \geq 0, \quad c_2 \geq 0, \quad c_n \geq 0$
WEC	$d_2 \geq 0, \quad c_{-1} \geq 0, \quad c_2 = 0, \quad n < 2, \quad c_n \geq 0$
SEC	$d_2 \leq 0, \quad c_{-1} \geq 0, \quad c_2 = 0, \quad n \leq 0 \cup n > 2, \quad c_n \geq 0$
DEC	$d_2 \geq 0, \quad c_{-1} \geq 0, \quad c_2 = 0, \quad -2 \leq n < 2, \quad c_n \geq 0$

**Table 2:** Sufficient conditions on the coefficients of the metric function  $B(r)$  for the classical energy criteria to be satisfied. Restrictions become increasingly stringent for stronger conditions. All four energy criteria are simultaneously fulfilled only in the very restricted setup with  $d_2 = 0$ ,  $c_{-1} \geq 0$ ,  $c_2 = 0$ , and the sum running over  $-2 \leq n \leq 0$  with  $c_n \geq 0$ .

The constraints imposed on the general metric function (2.43) by the classical energy conditions are summarized in Table 2. As expected, the SEC implies the NEC but not the WEC, while the DEC implies both the WEC and the NEC. Moreover, progressively stronger energy conditions lead to increasingly restrictive limitations on the metric.

## 3 Logarithmically corrected spacetime

In the previous section, we have set up a procedure for deriving NEC-fulfilling static and spherically symmetric metrics with  $A = 1/B$ , starting from Eqs. (2.33) and (2.34). Within the family of resulting geometries, we can single out a particularly relevant case by setting  $d_2 = 0$  in Eq. (2.38) (see also Eq. (2.41)). In this way, we obtain the asymptotically flat

spacetime featuring a logarithmic correction to the Schwarzschild solution

$$ds^2 = - \left[ 1 - \frac{R_S}{r} - \frac{c_{-1} r_d \ln(r/r_d)}{3r} \right] dt^2 + \left[ 1 - \frac{R_S}{r} - \frac{c_{-1} r_d \ln(r/r_d)}{3r} \right]^{-1} dr^2 + r^2 d\Omega^2, \quad (3.1)$$

where we have restored the length scale  $r_d$  for the upcoming discussion. By virtue of Einstein equations, this metric can be associated with the energy-momentum tensor

$$T_{\mu}{}^{\nu} = \frac{c_{-1} r_d}{24\pi r^3} \text{diag} \left( -1, -1, \frac{1}{2}, \frac{1}{2} \right), \quad (3.2)$$

which displays an anisotropic pressure distribution. Remarkably, one can verify that *all* energy criteria (2.7) are satisfied provided that  $c_{-1}$  is non-negative.

Interestingly, a line element of the form (3.1) also appears in Ref. [90], where it is used to study a phantom field as a dark-matter candidate in galactic environments, although the coefficient  $c_{-1}$  (corresponding to the parameter  $-a$  in Ref. [90]) is left arbitrary. Instead, our results furnish an additional theoretical restriction on the model by fixing the sign of  $c_{-1}$ . This highlights that our algorithm based on Eqs. (2.33) and (2.34) has a genuine physical foundation, as it permits the generation of metrics that arise in phenomenologically motivated scenarios while, at the same time, constraining their parameter space. Moreover, the logarithmic function in Eq. (3.1) involves two independent constants, as opposed to the single term used in Ref. [90]. As we will demonstrate below, this facet gives our framework a substantially richer structure.

In addition, logarithmic contributions also appear, for example, in generalized Bañados-Teitelboim-Zanelli (BTZ) black holes [91], in hairy black holes in Horndeski gravity [92], and in generic metric-affine frameworks [93]. Moreover, though the physical origin is different, logarithmic radial factors occur in the post-Newtonian (near-zone) expansion of the (harmonic-coordinate) metric (where they encode hereditary tails and tails-of-tails effects; see Eq. (87) in Ref. [94]). This property characterizes the so-called polyhomogeneous spacetimes in the context of radiating systems [95, 96].

In this section, we perform a detailed analysis of Eq. (3.1), which we regard as an effective static exterior geometry of a compact object, to be matched in principle to a (possibly regular) interior and intended to be valid in the domain probed by null and timelike geodesics. We begin by exploring its key features, such as the  $r = 0$  singularity (see Sec. 3.1) and the possible existence of horizon(s) (see Sec. 3.2). Afterwards, we carry out a preliminary assessment of the physical viability of this model. In Sec. 3.3, we discuss the emerge of photon spheres and innermost stable circular orbits (ISCOs), and compare our results with bounds provided by the Event Horizon Telescope (EHT) collaboration. In Sec. 3.4, we classify the horizonless and horizon-bearing configurations, while solar-system-like constraints are examined in Sec. 3.5. Finally, in Sec. 3.6 we evaluate junction conditions required to join the log-corrected solution to an exterior Schwarzschild spacetime.

### 3.1 The $r = 0$ singularity

The Ricci and Kretschmann scalars characterizing the log-metric (3.1) read as

$$\begin{aligned} R &= \frac{c_{-1}r_d}{3r^3}, \\ \mathcal{K} &= \frac{1}{9r^6} \left\{ 4c_{-1}r_d \ln(r/r_d) [3c_{-1}r_d \ln(r/r_d) - 5c_{-1}r_d + 18R_S] + 13(c_{-1}r_d)^2 \right. \\ &\quad \left. - 60c_{-1}r_d R_S + 108R_S^2 \right\}, \end{aligned} \quad (3.3)$$

respectively. Since they both blow as  $r \rightarrow 0^+$ , a curvature singularity is present at  $r = 0$ , where also the energy density (i.e.,  $-T_0^0$ ) blows up for any nonzero  $c_{-1}$  in view of Eq. (3.2).

In this regard, an intriguing feature of the spacetime is revealed by the study of the geodesic equation. Upon restricting to the equatorial plane  $\theta = \pi/2$ , it takes the form

$$\frac{1}{2} \left( \frac{dr}{d\lambda} \right)^2 + V_{\text{eff}} = \frac{E^2}{2}, \quad (3.4)$$

where the conserved energy  $E$  has been defined in Eq. (2.17) and

$$V_{\text{eff}} = \frac{1}{2} \left[ 1 - \frac{R_S}{r} - \frac{c_{-1}r_d \ln(r/r_d)}{3r} \right] \left( \frac{L^2}{r^2} + \alpha \right), \quad (3.5)$$

is the effective potential, where, for simplicity, we have adopted a different definition with respect to Eq. (2.27); in addition,

$$L \equiv r^2 \frac{d\phi}{d\lambda}, \quad (3.6)$$

is the conserved angular momentum associated with rotational symmetry, and, like before,  $\alpha = 1$  and  $\alpha = 0$  correspond to timelike and null geodesics, respectively.

Since  $c_{-1} > 0$  as required by the energy conditions,  $V_{\text{eff}} \rightarrow +\infty$  as  $r \rightarrow 0$ , except in the radial null case (i.e., when  $L = \alpha = 0$ ). This means that both timelike and non-radial null geodesics cannot reach the singularity, unlike radial null rays.

### 3.2 Horizon structure

Since we are dealing with a static and spherically symmetric geometry, the locations of possible horizons are determined by the condition

$$B(r_h) = 1 - \frac{R_S}{r_h} - \frac{c_{-1}r_d \ln(r_h/r_d)}{3r_h} = 0, \quad (3.7)$$

which yields the solution

$$r_h = -\frac{c_{-1}r_d}{3} W_k \left[ -\frac{3}{c_{-1}} e^{-3R_S/(c_{-1}r_d)} \right]. \quad (3.8)$$

Here,  $W_k$  denotes the  $k$ -th branch of the (multivalued) Lambert  $W$  function [97, 98], implicitly defined by the relation

$$W(x)e^{W(x)} = x. \quad (3.9)$$

When the argument  $x$  is real, only the two real-valued branches  $W_0$  and  $W_{-1}$  (referred to as principal and lower branches, respectively) are relevant, and thus Eq. (3.9) admits the following structure:

- $x \geq 0$ : there exists exactly one real root, namely  $W_0$ ;
- $-1/e < x < 0$ : two *distinct* and real solutions occur, i.e.,  $W_0$  and  $W_{-1}$ ;
- $x = -1/e$ : the two real branches  $W_0$  and  $W_{-1}$  merge into a single degenerate value, owing to the identity  $W(-1/e) = -1$ ;
- $x < -1/e$ : no real solutions are possible.

Therefore, the presence of the Lambert  $W$  function in formula (3.8) entails that the space-time may exhibit two horizons, a single horizon (which we can view as an extremal horizon, since the two horizons associated with  $W_0$  and  $W_{-1}$  coalesce), or no horizon at all. We now investigate this point in detail.

From Eq. (3.8), we see that it is convenient to express the argument of  $W$  in terms of the  $c_{-1}$ -dependent function

$$x(c_{-1}) = -\frac{3}{c_{-1}} e^{-3R_S/(c_{-1}r_d)}, \quad (3.10)$$

which, under our assumptions (recall that  $c_{-1}$ ,  $R_S$ , and  $r_d$  are positive) is always negative and attains a minimum at

$$c_{-1,\min} = \frac{3R_S}{r_d}, \quad (3.11a)$$

where

$$x_{\min} = -\frac{r_d}{R_S e}. \quad (3.11b)$$

As  $c_{-1} \rightarrow 0^+$  or  $c_{-1} \rightarrow \infty$ ,  $x(c_{-1})$  approaches zero from below, and thus its overall range is

$$x(c_{-1}) \in [x_{\min}, 0), \quad (3.12)$$

where we have excluded  $x(c_{-1}) = 0$ , because it would give  $r_h = 0$  in Eq. (3.8) due to the fact that the Lambert function satisfies  $W(0) = 0$ .

Now, taking into account the properties of  $W$  discussed above and the fact that  $r_d$  is *a priori* a free parameter, we can distinguish the following situations:

- $r_d < R_S$ . From Eq. (3.11b), one has  $x_{\min} > -1/e$ . By Eq. (3.12), this implies that  $x(c_{-1}) > -1/e \forall c_{-1} > 0$ , which reveals that the argument of the Lambert function always lies in the interval where both real branches  $W_0$  and  $W_{-1}$  exist. Consequently, for any  $c_{-1} > 0$ , the spacetime (3.1) always supports two horizons.

- $r_d = R_S$ . In this case, Eq. (3.11) indicates that the function  $x(c_{-1})$  takes at  $c_{-1,\min} = 3$  the minimum  $x_{\min} = -1/e$ . Therefore, when  $c_{-1} = 3$ , the branches  $W_0$  and  $W_{-1}$  coincide, giving rise to a single (degenerate) horizon located at  $r = R_S$ . For  $c_{-1} \neq 3$ , we have  $x(c_{-1}) > -1/e$ , and hence the metric develops two horizons, one of which always at  $r = R_S$ . In particular, for  $c_{-1} < 3$ ,  $r = R_S$  corresponds to the outer horizon.
- $r_d > R_S$ . Since  $x_{\min} < -1/e$ , the metric may allow for two, one, or no horizon, depending on the value of  $c_{-1}$ . In this latter scenario,  $r = 0$  becomes a naked singularity.

### 3.3 Photon spheres and innermost stable circular orbits

The radii of circular orbits traced by photons are obtained by solving  $\partial V_{\text{eff}}^{\text{null}}/\partial r = 0$ , where the “null” effective potential  $V_{\text{eff}}^{\text{null}}$  can be read off from Eq. (3.5) with  $\alpha = 0$ . This relation yields

$$6r + c_{-1}r_d - 9R_S - 3c_{-1}r_d \ln(r/r_d) = 0, \quad (3.13)$$

whose solutions is

$$r_{\text{ps}} = -\frac{c_{-1}r_d}{2} W_k \left\{ -\frac{2}{c_{-1}} e^{[1/3 - 3R_S/(c_{-1}r_d)]} \right\}, \quad (3.14)$$

the argument of  $W$  defining

$$x(c_{-1}) = -\frac{2}{c_{-1}} e^{[1/3 - 3R_S/(c_{-1}r_d)]}. \quad (3.15)$$

The function  $x(c_{-1})$  is always negative (since  $c_{-1}$  is positive), and satisfies  $x(c_{-1}) \rightarrow 0^-$  as  $c_{-1} \rightarrow 0^+$  or  $c_{-1} \rightarrow \infty$ . The minimum occurs at  $c_{-1} = 3R_S/r_d$ , where

$$x_{\min} = -\frac{2r_d}{3R_S e^{2/3}}, \quad (3.16)$$

implying that the range is

$$x(c_{-1}) \in [x_{\min}, 0). \quad (3.17)$$

Therefore, following a similar analysis as in Sec. 3.2, there may be one, two, or no solutions of Eq. (3.13), depending on the value of  $c_{-1}$  and the ratio  $r_d/R_S$ . Typically, the maximum of the effective potential corresponds to the (unstable) photon sphere, while the minimum defines what is known as the stable photon sphere, sometimes also referred to as the anti-photon sphere [99]. To avoid confusion, throughout the paper we use the term “photon sphere” simply to refer to a real solution of Eq. (3.13). However, in configurations supporting horizon(s), one should recall that only the root lying outside the (outer) event horizon is physically relevant. This follows from the fact that photon spheres are timelike hypersurfaces, while inside the (outer) horizon they become spacelike (equivalently, inside the outer horizon the coordinates  $r$  and  $t$  exchange their role). By taking  $r_d = R_S$ , Fig. 1 provides a visual summary of the geometry by showing how the photon sphere radius  $r_{\text{ps}}$  varies with  $c_{-1}$ , with the corresponding horizon radii  $r_h^{\text{outer}}$  and  $r_h^{\text{inner}}$  (cf. Eq. (3.8)) also displayed for comparison.

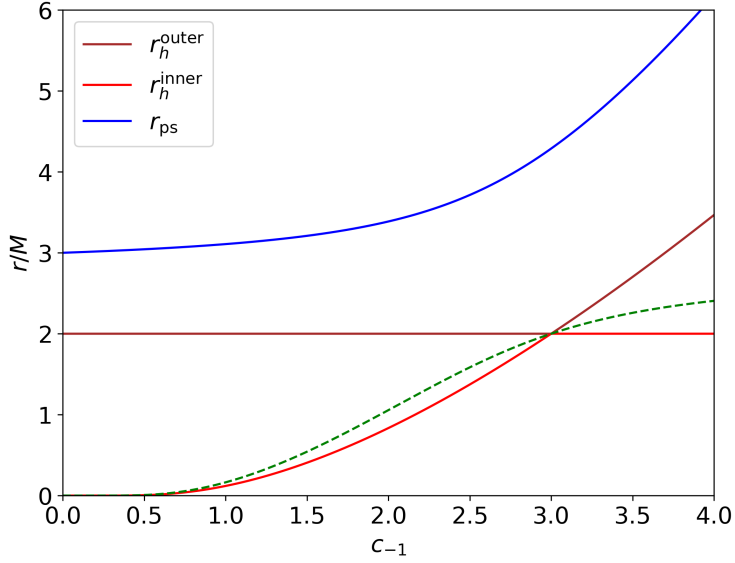


**Figure 1:** Outer and inner horizon radii,  $r_h^{outer}$  and  $r_h^{inner}$ , and the photon sphere radius  $r_{ps}$  as functions of the parameter  $c_{-1}$  in the scenario with  $r_d = R_S$ . The green dashed line corresponds to the second root of Eq. (3.13), which lies between the inner and the outer horizons. This solution does not identify a physical photon sphere, as such a surface must be timelike.

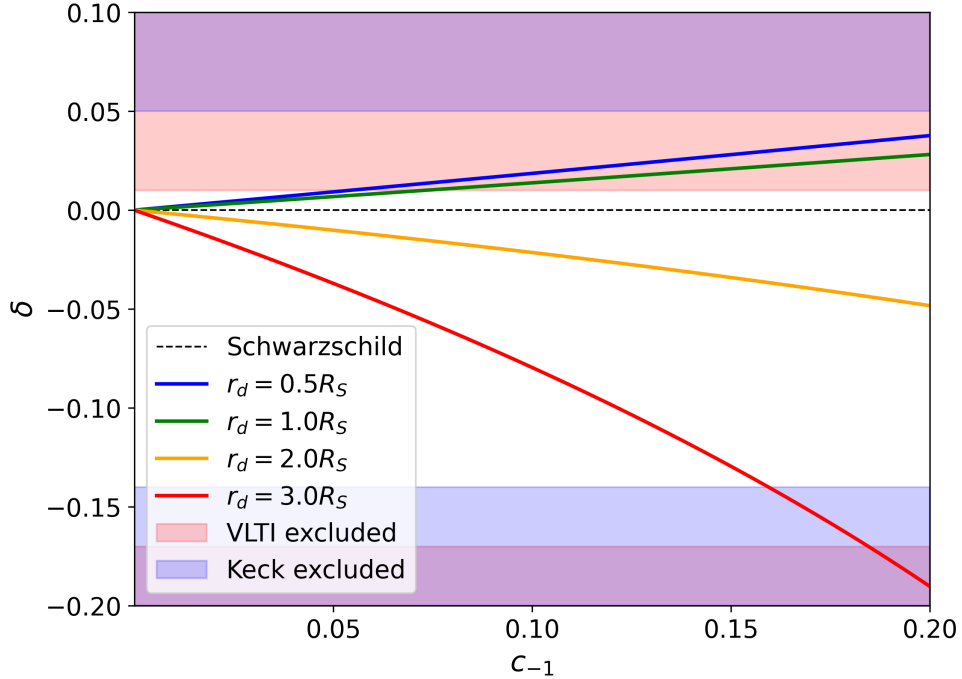


**Figure 2:** Fractional shadow diameter deviation from the Schwarzschild solution as a function of  $c_{-1}$  for different values of the characteristic radius  $r_d$ . The white region is consistent with the EHT observations of Sgr A\*. The geometry (3.1) is allowed by empirical constraints for certain ranges of  $c_{-1}$ .

The apparent radius of the photon sphere, typically used to characterize the shadow of a black hole [100–106], is given by the critical impact parameter [107–109]<sup>4</sup>:

$$b_c = \frac{r_{\text{ps}}}{\sqrt{B(r_{\text{ps}})}}, \quad (3.18)$$

where, as usual,  $b := L/E$ . Defining the fractional deviation parameter as [111]

$$\delta := \frac{b_c}{b_c^{\text{S}}} - 1, \quad (3.19)$$

with  $b_c^{\text{S}} = 3\sqrt{3}M$  serving as the Schwarzschild benchmark [19], one can then constrain the factor  $c_{-1}$  by comparing the predicted values of  $\delta$  with the EHT observations of Sgr A\*. The result is presented in Fig. 2, where the shaded regions are ruled out by the Keck (blue,  $\delta = -0.04_{-0.10}^{+0.09}$ ) and VLTI (red,  $\delta = -0.08_{-0.09}^{+0.09}$ ) priors [111].

Remarkably, the logarithmically corrected spacetime (3.1) is not excluded by current data and hence can potentially represent a physically viable model.

Another relevant scale is defined by the ISCO radius, which plays an important role in the accretion dynamics of compact objects (see e.g. Refs. [112, 113]). Following a similar procedure as before, and imposing that the first and second derivatives of the effective potential (3.5) with  $\alpha = 1$  vanish, we find that  $r_{\text{ISCO}}$  satisfies

$$\begin{aligned} & -3c_{-1}^2 r_d^2 \ln^2(r_{\text{ISCO}}/r_d) - 2c_{-1}^2 r_d^2 + c_{-1} r_d \ln(r_{\text{ISCO}}/r_d) (4c_{-1} r_d + 3r_{\text{ISCO}} - 18R_{\text{S}}) \\ & + 12c_{-1} r_d R_{\text{S}} + 9R_{\text{S}} (r_{\text{ISCO}} - 3R_{\text{S}}) = 0, \end{aligned} \quad (3.20)$$

which, to first order in  $c_{-1}$ , yields

$$r_{\text{ISCO}} = 3R_{\text{S}} + c_{-1} r_d \left[ \ln \left( \frac{3R_{\text{S}}}{r_d} \right) - \frac{4}{3} \right] + \mathcal{O}(c_{-1}^2). \quad (3.21)$$

### 3.4 Classification of horizon-bearing and horizonless configurations

Since the log-metric (3.1) satisfies all standard energy conditions and is not ruled by EHT data, it is natural to ask whether it can describe the exterior domain of a horizonless compact object which, in some regime, acts as a black hole mimicker, or whether it can instead be associated with a new black hole model. In this latter situation, following the terminology adopted in Ref. [114], we may refer to it as a “*bona fide*” black hole, characterized by an (outer) horizon and a single (physical) unstable photon sphere.

By contrast, a wide class of horizonless ultra-compact black hole mimickers typically display two light rings: an outer unstable photon sphere and an inner stable one (the anti-photon sphere) [28, 99, 115, 116]. This intriguing setup naturally leads to a branch

---

<sup>4</sup>In non-asymptotically flat spacetimes, the critical impact parameter alone is insufficient to fully characterize the observable angular structure [110]; instead, one should compute the apparent angle for an observation at a finite radius. Although our metric does not possess a finite ADM mass, it still approaches the Minkowski form at spatial infinity. Hence, it is valid to use the critical impact parameter alone to study the shadow.

structure, with distinct observational consequences for lensing and shadow formation [99], as well as long-lived photon trapping and enhanced time-delay effects, which may be relevant for echo-like features in both electromagnetic and gravitational signals [117].

Introducing the dimensionless parameter

$$X := \frac{3R_S}{c_{-1}r_d} > 0, \quad (3.22)$$

the arguments of the Lambert  $W$  functions in Eqs. (3.8) and (3.14) can be recast, respectively, as

$$x_h = -\frac{3}{c_{-1}}e^{-X}, \quad (3.23)$$

$$x_{\text{ps}} = -\frac{2}{c_{-1}}e^{(\frac{1}{3}-X)}. \quad (3.24)$$

Recalling that  $W(x)$  attains real values only for  $x \in [-1/e, 0)$ , the existence of a real photon sphere radius entails that

$$\frac{2}{c_{-1}}e^{(\frac{1}{3}-X)} \leq \frac{1}{e}, \quad (3.25)$$

while the absence of an event horizon is ensured by

$$\frac{3}{c_{-1}}e^{-X} > \frac{1}{e}. \quad (3.26)$$

Combining inequalities (3.25) and (3.26), we obtain that the allowed range of  $r_d$  for a fixed  $R_S$  is

$$\frac{3R_S}{c_{-1} \left[ \ln\left(\frac{3}{c_{-1}}\right) + 1 \right]} < r_d \leq \frac{3R_S}{c_{-1} \left[ \ln\left(\frac{2}{c_{-1}}\right) + \frac{4}{3} \right]}. \quad (3.27)$$

Remarkably, within this interval, the spacetime exhibits one or two photon spheres while remaining horizonless.

The phase diagram in the  $(c_{-1}, r_d/R_S)$  parameter space is presented in Fig. 3, while a classification of the potential configurations realized is presented in Table 3.

Horizon-bearing structures possess the key properties to be qualified as “*bona fide*” black holes. Although they always exhibit two extrema of the “null” effective potential  $V_{\text{eff}}^{\text{null}}$ , only one corresponds to a genuine photon sphere, since the other lies inside the horizon and is thus unphysical. Moreover, in geometries with two horizons the outer one is located, in many cases, at  $r = R_S$  or in its vicinity, the latter scenario arising for sufficiently small values of  $c_{-1}$  and arbitrary  $r_d$  (cf. Eq. (3.8)). This black-hole-like pattern is compatible with the occurrence of the  $r = 0$  singularity studied in Sec. 3.1, so the matching to a regular interior could be avoided.<sup>5</sup>

On the other hand, horizonless models can be classified as members of a new class of compact bodies, which we can dub “non-exotic compact objects” to stress that they respect all classical energy criteria and hence differ from many familiar exotic compact-objects

---

<sup>5</sup>In Ref. [118], we will present a detailed discussion on regular geometries, some of which admit regular metrics with logarithmic corrections.

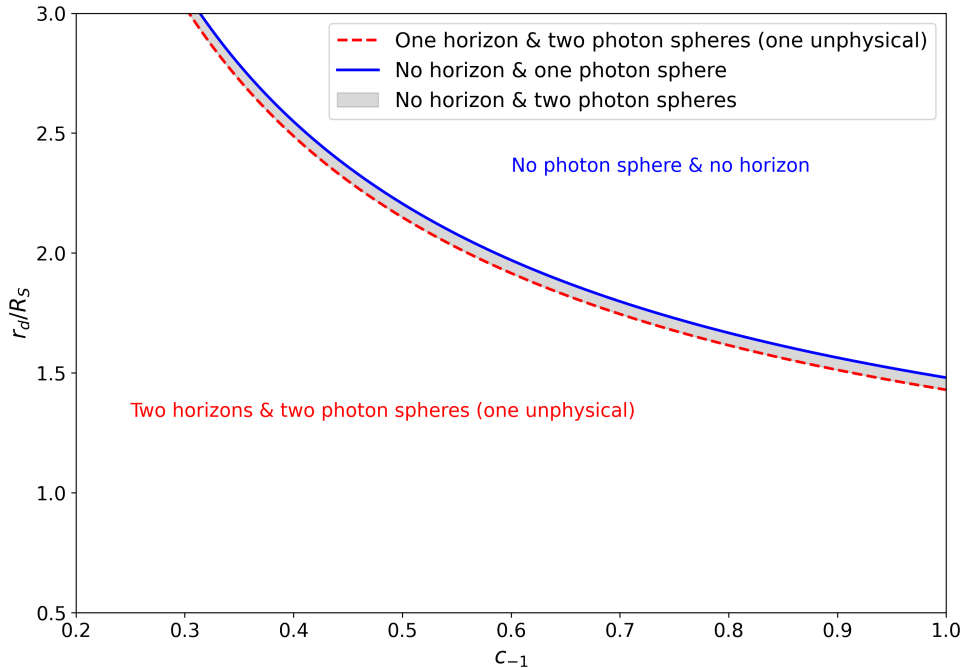


**Figure 3:** Phase diagram in the  $(c_{-1}, r_d/R_S)$  parameter space for the logarithmically corrected geometry (3.1). The red dashed line separates configurations with two horizons (below) and no horizon (above), while the blue solid line marks the boundary between solutions with two photon spheres (below) and no photon sphere (above). The gray shaded region corresponds to horizonless objects with two photon spheres, which have the key geometric features required to serve as black hole mimickers.

proposals (e.g., traversable wormholes or gravastars) that often require energy-condition violations or rely on quantum effects near the surface [28]. Horizonless setups supporting two light rings are characterized by an unstable outer photon sphere and a stable inner anti-photon sphere. These frameworks can thus potentially act as black hole mimickers, provided that they reproduce the exterior phenomenology of a black hole at the level of observables. This construction requires, as pointed out before, interpreting the log-corrected metric as an effective exterior geometry joined to a regular interior that removes the (naked)  $r = 0$  singularity, which can nonetheless be reached only by radial null geodesics (see Sec. 3.1). This viewpoint also facilitates drawing a parallel with exotic compact objects, many of which are explicitly designed to avoid a singular central region by means of similar matching prescriptions.

In order to further explore the possibility of associating the solution (3.1) with the description of compact objects, we recall that the compactness of a gravitating body with mass  $\mathcal{M}$  and finite characteristic radius  $R$  is conventionally defined as  $\mathcal{C} := \mathcal{M}/R$  [119]. Configurations with  $\mathcal{C} \sim O(1)$  are typically regarded as highly compact [32] (e.g., for neutron stars one generally finds  $\mathcal{C} \sim 0.2$ , which is orders of magnitude higher than the solar-system benchmark value  $\mathcal{C} \sim 10^{-6}$  [119]), although in general relativity the Buchdahl theorem imposes the upper bound  $\mathcal{C} \leq 4/9$  [28]. Based on the taxonomy outlined in Ref. [28],

Configuration	Model
One horizon, two photon spheres	“ <i>Bona fide</i> ” black hole
Two horizons, two photon spheres	“ <i>Bona fide</i> ” black hole
No horizon, two photon spheres	Black hole mimicker
No horizon, one photon sphere	“Non-exotic compact object”
No horizon, no photon sphere	“Non-exotic compact object”

**Table 3:** Classification of the logarithmically corrected solution (3.1) according to the horizon structure and photon-sphere properties, which are considered in Fig. 3. Models featuring one or two horizons and two photon spheres (only one of which is physical) exhibit the geometric properties associated with “*bona fide*” black holes. Horizonless configurations possessing both an unstable and a stable photon sphere can be qualified as black hole mimickers, while horizonless solutions with one or no photon sphere can act as “non-exotic compact objects”, as they do not involve violations of classical energy conditions.

our log-geometry displays the essential characteristics to pertain to compact or even ultra-compact objects, as it admits an ISCO that can be located at  $r_{\text{ISCO}} \sim 3R_{\text{S}}$  (cf. Eq. (3.21)) and a photon sphere whose radius can be read off from Eq. (3.14) (see Fig. 1 for the case  $r_d = R_{\text{S}}$  in horizon-bearing setups).

An additional indicator of high compactness fulfilled by the log-metric is the existence of infinite-redshift surfaces or *nearly* infinite-redshift surfaces (see e.g. Refs. [30, 83] and references therein). To illustrate this point, we focus on the special parameter choice for which the metric function  $B(r)$  admits a degenerate zero at  $r = r_h$ , namely

$$B(r_h) = 0, \quad B'(r_h) = 0. \quad (3.28)$$

Solving these conditions yields

$$c_{-1} = \frac{3r_h}{r_d}, \quad r_h \left[ 1 - \ln\left(\frac{r_h}{r_d}\right) \right] = R_{\text{S}}, \quad (3.29)$$

indicating that  $r = r_h$  is a double root of  $B(r)$ . Consequently, the redshift factor  $z$  for signals emitted by static sources approaching  $r_h$  diverges as

$$z \sim B(r)^{-1/2} \longrightarrow \infty, \quad r \rightarrow r_h^+. \quad (3.30)$$

Thus,  $r = r_h$  corresponds to an infinite-redshift surface (recall that the event horizon of a static, spherically symmetric spacetime is automatically an infinite-redshift surface). Conversely, scenarios where  $B(r)$  never vanishes but can be arbitrarily close to zero (as

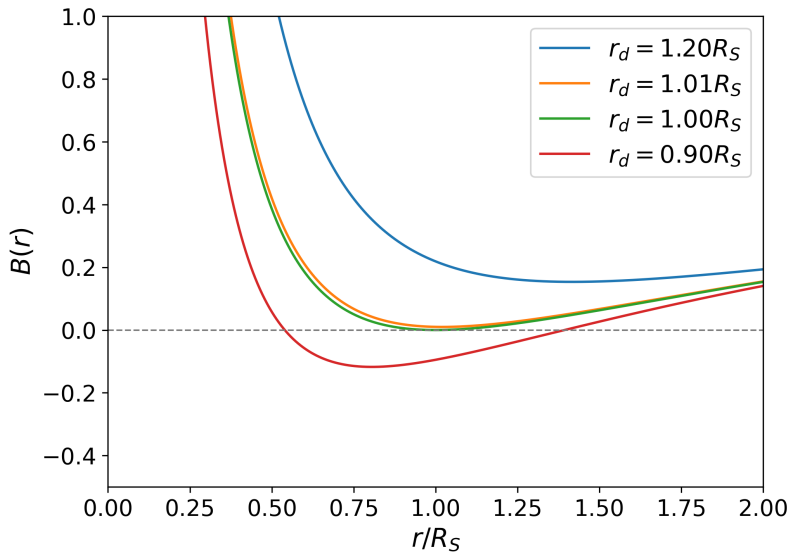


**Figure 4:** The metric function  $B(r)$  for the logarithmically corrected spacetime with fixed  $c_{-1} = 3$  and selected representative values of the scale parameter  $r_d$ . The threshold case  $r_d = R_S$  (green curve) corresponds to a degenerate root at  $r = r_h$  (cf. Eq. (3.28)), signaling the emergence of an infinite-redshift surface. Small deviations from this limiting scenario remove the degeneracy and either produce a “*bona fide*” black hole with two horizons (red curve), or lead to a nearly infinite-redshift surface (more pronounced for the orange curve and slightly less for the blue curve), thereby maintaining the high compactness of the configuration.

displayed by the orange curve and, to a lesser extent, by the blue curve in Fig. 4) give rise to horizonless patterns with a nearly infinite-redshift surface at  $r = r_z$ . In these cases, the exact relations (3.28) are no longer strictly satisfied, but one finds

$$B(r_z) \rightarrow 0^+, \quad B'(r_z) = 0, \quad (3.31)$$

which describe signals experiencing extremely large, albeit finite, gravitational redshift at  $r = r_z$ . The behavior of  $B(r)$  for  $c_{-1} = 3$  is shown in Fig. 4, which illustrates that the geometry allows for both infinite- and nearly infinite-redshift surfaces.

Some final remarks are now in order. Another significant facet supporting the interpretation of Eq. (3.1) as a suitable effective exterior geometry is that this metric is unlikely to originate from standard gravitational-collapse processes, for at least two reasons: (i) timelike geodesics are prevented from reaching  $r = 0$ ; (ii) this curvature singularity persists also in the absence of an event horizon (see Sec. 3.1). Moreover, at this stage, the solution should be regarded as a *geometric* rather than astrophysical candidate for a new family of compact bodies, possibly including black hole mimickers. Our analysis is indeed meant to be preliminary, since key quantities such as the closeness parameter, as well as important aspects like formation and stability mechanisms, have not yet been assessed [28, 120–124]. Nonetheless, our examination shows that Eq. (3.1) contains all the essential ingredients

for modeling such compact configurations, providing further evidence that the algorithm devised in Sec. 2.2.1, based on Eqs. (2.33) and (2.34), has a solid physical grounding.

### 3.5 Constraints from solar-system-like environments

In the spirit of treating the log-corrected spacetime as an effective exterior geometry, we now investigate bounds on  $c_{-1}$  stemming from solar-system-like environments, which probe the metric in the weak-field regime and hence are insensitive to its behavior at small radii or to the details of a possible interior completion. From this perspective, all constraints derived here should not be interpreted as fundamental theoretical restrictions on the model, nor do they supersede the less stringent limitations provided by EHT observations discussed in Sec. 3.3.

We begin by analyzing the gravitational redshift in Sec. 3.5.1. Then, the bending of light and the orbit precession are explored in Secs. 3.5.2 and 3.5.3, respectively.

In this section, we set the length scale  $r_d$  to be equal to  $R_S$ .

#### 3.5.1 Gravitational redshift

The gravitational redshift relates the emitted and received frequencies,  $\omega_1$  and  $\omega_2$ , for two static observers located at radii  $r_1$  and  $r_2$ , via [19]

$$\frac{\omega_1}{\omega_2} = \frac{\sqrt{B(r_2)}}{\sqrt{B(r_1)}}. \quad (3.32)$$

In the limit  $R_S/r \ll 1$ , we find

$$\begin{aligned} \frac{1}{B(r)} = & 1 + \frac{[3 + c_{-1} \ln(r/R_S)]R_S}{3r} \\ & + \frac{[9 + 6c_{-1} \ln(r/R_S) + 2c_{-1}^2 \ln(r/R_S)]R_S^2}{9r^2} + \dots, \end{aligned} \quad (3.33)$$

where we have regarded  $\ln(r/R_S)$  as a zeroth-order term in the expansion in  $R_S/r$ . At leading order, the fractional frequency shift  $\delta_\omega := (\omega_2 - \omega_1)/\omega_1$  becomes

$$\delta_\omega \approx \Phi(r_1) - \Phi(r_2), \quad (3.34)$$

where  $\Phi$  is the effective Newtonian gravitational potential in the weak-field limit:

$$\Phi = \frac{B(r) - 1}{2} = -\frac{R_S}{2r} \left[ 1 + \frac{c_{-1} \ln(r/R_S)}{3} \right]. \quad (3.35)$$

Owing to Eq. (3.34), the following relation for  $c_{-1}$  can be derived:

$$c_{-1} = \frac{3[2r_1r_2\delta_\omega + R_S(r_2 - r_1)]}{R_S[r_1 \ln(r_2/R_S) - r_2 \ln(r_1/R_S)]}. \quad (3.36)$$

The gravitational redshift has been experimentally confirmed with an accuracy of approximately  $2 \times 10^{-4}$  by the space-based experiment Gravity Probe A [125], assuming the Schwarzschild solution. Taking  $r_1$  to be the Earth radius  $R_\oplus \approx 6371$  km,  $R_S \approx 8.87 \times 10^{-6}$  km the corresponding Schwarzschild radius, and  $r_2 \approx 16371$  km the radial coordinate of the receiver located at an altitude of about 10000 km above the Earth surface (reflecting the standard setup used in Gravity Probe A tests [125]), we arrive at the solar system constraint

$$c_{-1}|_{\text{solar system}}^{\text{redshift}} \lesssim 3.03 \times 10^{-5}. \quad (3.37)$$

### 3.5.2 Bending of light

Starting from the geodesic equations (3.4) and (3.5) with  $\alpha = 0$ , together with the definition (3.6) of angular momentum, one can easily show that the spatial orbit of a photon in the equatorial plane of the spacetime (3.1) is governed by

$$\frac{d\phi}{dr} = \pm \frac{1}{r^2} \left[ \frac{1}{b^2} - \frac{B(r)}{r^2} \right]^{-1/2}, \quad (3.38)$$

where we recall  $b := L/E$  and the upper (resp. lower) sign refers to clockwise (resp. counterclockwise) motion.

The deflection of the light trajectory from a straight line is defined as  $\delta\phi := \Delta\phi - \pi$ , where  $\Delta\phi \equiv |\phi_{+\infty} - \phi_{-\infty}|$  is the total change of the angular coordinate  $\phi$ , with  $\phi_{-\infty}$  and  $\phi_{+\infty}$  the asymptotic values along the incoming and outgoing photon paths, respectively. Since at the distance of closest approach  $r_0$  the quantity  $dr/d\phi$  vanishes, Eq. (3.38) gives

$$b^2 = \frac{r_0^2}{B(r_0)}, \quad (3.39)$$

and hence, by expanding the integrand of the relation  $\Delta\phi = 2 \int_{r_0}^{\infty} dr r^{-2} [B(r_0)/r_0^2 - B(r)/r^2]^{-1/2}$  in the small parameter  $R_S/r$ , we obtain, upon neglecting higher-order contributions,

$$\begin{aligned} \Delta\phi = & 2 \int_{r_0}^{\infty} \frac{dr}{r [r^2/r_0^2 - 1]^{1/2}} \left[ 1 + \frac{(r^2 + rr_0 + r_0^2)R_S}{2r_0(r + r_0)r} \right. \\ & \left. + \frac{c_{-1} [r^3 \ln(r_0/R_S) - r_0^3 \ln(r/R_S)] R_S}{6r_0 (r^2 - r_0^2) r} + \dots \right]. \end{aligned} \quad (3.40)$$

Performing the integral yields

$$\delta\phi = \frac{2R_S}{r_0} \left[ 1 + \frac{c_{-1}}{3} \ln \frac{r_0}{2R_S} \right] + \dots, \quad (3.41)$$

which translates into the general expression for the coefficient  $c_{-1}$ :

$$c_{-1} = \frac{3}{\ln(r_0/2R_S)} \left( \frac{r_0\delta\phi}{2R_S} - 1 \right). \quad (3.42)$$

In the case of a light ray grazing the solar surface, we can use  $R_S \approx 2.95$  km and  $r_0 = R_\odot \approx 6.96 \times 10^5$  km. Since very-long-baseline interferometry measurements agree with the general-relativistic prediction  $2R_S/R_\odot$  to an accuracy of 0.01 % [125], we can conclude from Eq. (3.42) that

$$c_{-1}|_{\text{solar system}}^{\text{light bending}} \lesssim 2.57 \times 10^{-5}. \quad (3.43)$$

### 3.5.3 Orbit precession

In the previous section, we have dealt with the unbounded trajectories of photons. We now turn to the bound orbits of massive particles around a central object. Following standard arguments [126], one finds that this motion is ruled by

$$\left(\frac{d\mu}{d\phi}\right)^2 + B\left(\mu^2 + \frac{4L^2}{R_S^2}\right) = \frac{4E^2L^2}{R_S^2}, \quad (3.44)$$

where we have introduced the dimensionless parameter [127]

$$\mu := \frac{2L^2}{R_S r}. \quad (3.45)$$

Differentiating Eq. (3.44) with respect to  $\phi$  in the limit  $R_S/r \sim \mu R_S^2/L^2 \ll 1$ , we obtain, for our explicit form of  $B$  given in Eq. (3.1),

$$\frac{d^2\mu}{d\phi^2} + \mu - 1 = h(\mu, R_S, c_{-1}), \quad (3.46)$$

where the function

$$h(\mu, R_S, c_{-1}) \equiv \frac{3R_S^2\mu^2}{4L^2} - \frac{c_{-1}}{3} \ln\left(\frac{\mu R_S^2}{2L^2}\right) + \dots, \quad (3.47)$$

collects the leading relativistic and logarithmic corrections. In Newtonian gravity, where  $h$  vanishes, we get a solution describing a perfect ellipse with eccentricity  $e$ :

$$\mu_0 = 1 + e \cos \phi. \quad (3.48)$$

We can thus assume the perturbative expansion of  $\mu$

$$\mu = \mu_0 + \mu_1, \quad (3.49)$$

where  $\mu_1$  represents a small deviation from the Newtonian trajectory  $\mu_0$ . Substituting this *ansatz* into Eq. (3.46) and retaining only first-order corrections in  $\mu_1$ , we obtain

$$\frac{d^2\mu_1}{d\phi^2} + \mu_1 = h(\mu_0, R_S, c_{-1}), \quad (3.50)$$

which admits an analytical solution, although the full expression is rather lengthy. For our purposes, the most relevant term is the non-constant and non-periodic (dominant secular) contribution

$$\mu_1 = \left( \frac{3eR_S^2}{4L^2} - \frac{c_{-1}}{3e} \right) \phi \sin \phi + \dots, \quad (3.51)$$

governing the cumulative precession. Therefore, the orbit is described by

$$\mu = 1 + e \cos \phi + \left( \frac{3R_S^2}{4L^2} - \frac{c_{-1}}{3e^2} \right) e \phi \sin \phi. \quad (3.52)$$

If we introduce the small parameter

$$\gamma := \frac{3R_S^2}{4L^2} - \frac{c_{-1}}{3e^2}, \quad (3.53)$$

then Eq. (3.52) can be formulated as an ellipse with a period different from  $2\pi$ :

$$\mu = 1 + e \cos [(1 - \gamma)\phi], \quad (3.54)$$

and thus the perihelion precession per orbit is given by  $\Delta\phi_{\text{prec}} = 2\pi\gamma$ . Bearing in mind the standard polar equation of the ellipse with semi-major axis  $a$

$$r(\phi) = \frac{(1 - e^2)a}{1 + e \cos \phi}, \quad (3.55)$$

jointly with the definition of  $\mu$  from Eq. (3.45) and the zero-order solution (3.48), we arrive at the approximate formula for the angular momentum

$$L^2 \approx a(1 - e^2)R_S/2. \quad (3.56)$$

The perihelion advance per orbit then reads as

$$\Delta\phi_{\text{prec}} = \frac{3\pi R_S}{(1 - e^2)a} \Lambda, \quad (3.57)$$

where the dimensionless parameter  $\Lambda$  encodes departures from standard Schwarzschild metric

$$\Lambda \equiv 1 - \frac{2c_{-1}a(1 - e^2)}{9e^2R_S}, \quad (3.58)$$

which solving for  $c_{-1}$  leads to

$$c_{-1} = \frac{(1 - \Lambda)9e^2R_S}{2a(1 - e^2)}. \quad (3.59)$$

This formula facilitates direct comparison with established post-Newtonian constraints. Using the results from Refs. [128–130]

$$\Lambda = 1.003 \pm 0.005, \quad (3.60)$$

together with relevant orbital elements of Mercury,  $a \simeq 5.79 \times 10^7$  km and  $e = 0.2056$  [126], we infer the limit

$$c_{-1}|_{\text{solar system}}^{\text{precession}} \lesssim 2.02 \times 10^{-11}. \quad (3.61)$$

Apart from the above weak-field solar-system bound, a complementary mid-field constraint can be obtained from the relativistic precession of the S2 star orbiting Sgr A\*, for which the GRAVITY Collaboration has reported a perihelion advance of approximately  $12'$  per orbital period [131]. Following Ref. [131], which neglects Kerr spin effects, deviations from the Schwarzschild prediction can be quantified via the dimensionless parameter  $\Lambda_{\text{S2}}$  (denoted by  $f_{\text{SP}}$  in Ref. [131]), whose established value is

$$\Lambda_{\text{S2}} = 1.10 \pm 0.19. \quad (3.62)$$

Using the S2 orbital parameters  $a \simeq 125 R_{\text{S}}$  and  $e \simeq 0.885$  [131], Eq. (3.59) yields the bound

$$c_{-1}|_{\text{S2}}^{\text{precession}} \lesssim 0.0117, \quad (3.63)$$

which is several orders of magnitude weaker than the solar-system limit (3.61). The milder constraint suggests that the log-corrected geometry (3.1) is potentially more relevant for describing galactic environments than the solar system. Importantly, the bound (3.63) lies entirely within the parameter region allowed by EHT observations of Sgr A\*, as illustrated in Fig. 2.

### 3.6 Junction conditions

Although asymptotically flat (cf. Eq. (2.15)), the Misner-Sharp-Hernandez mass  $\mathcal{M} = \frac{r}{2}(1 - \nabla^\mu r \nabla_\mu r)$  associated with the spacetime (3.1) grows logarithmically and hence diverges at infinity, a behavior known to be pathological for isolated systems [57] (in other words, the metric is not asymptotically Schwarzschild in the standard “isolated system” sense). To cure this issue and give a consistent physical interpretation to the model, we assume, in line with its effective character, that beyond some large radius  $\mathcal{R} > 2M_\infty$  the geometry is joined to an exterior Schwarzschild region

$$ds_{\text{S}}^2 = - \left(1 - \frac{2M_\infty}{r}\right) dt^2 + \left(1 - \frac{2M_\infty}{r}\right)^{-1} dr^2 + r^2 d\Omega^2. \quad (3.64)$$

Let  $\Sigma$  be the timelike hypersurface  $r = \mathcal{R}$ , where we install the intrinsic coordinates  $y^A = (\tau, \theta, \phi)$  (here, capital Latin indices  $A, B = 1, 2, 3$ ), with  $\tau$  the proper time of static observers on  $\Sigma$ . Then, following the general recipe of the Israel-Lanczos formalism [3, 4], we find that the first Darmois junction condition, i.e., the induced three-metric  $h^{AB}$  having no jump discontinuity across  $\Sigma$ , requires that temporal (and thus radial) metric components be the same on both sides of  $\Sigma$ , which thus yields the relation (recall that  $R_{\text{S}} \equiv 2M$ )

$$M_\infty = M + \frac{c_{-1} r_d}{6} \ln(\mathcal{R}/r_d). \quad (3.65)$$

Therefore,  $M_\infty$  represents the ADM mass, i.e., the total physical (“renormalized”) mass measured at infinity by an asymptotic observer after the matching has been performed. On the other hand,  $M$  can be regarded as an effective (“bare”) interior mass associated with the pure  $1/r$  contribution to  $B(r)$ . This parameter is involved in the description of the gravitational field (it enters, for instance, the equations determining the horizons, photon spheres, and ISCOs) in the exterior region  $\mathcal{R}_0 < r < \mathcal{R}$ , where  $\mathcal{R}_0$  denotes the radius of the inner (possibly regular) completion. For instance, in the solar-system-like environments considered in Sec. 3.5, the difference between  $M_\infty$  and  $M$  can be extremely small as  $c_{-1} \ll 1$ .

The second junction condition, i.e., continuity of the extrinsic curvature, demands the equality of the radial derivatives of temporal metric components at  $\Sigma$ . This criterion is not fulfilled owing to the mismatch

$$\left(1 - \frac{2M_\infty}{r}\right)' \Big|_\Sigma - \left(1 - \frac{2M}{r} - \frac{c_{-1}r_d \ln(r/r_d)}{3r}\right)' \Big|_\Sigma = \frac{c_{-1}r_d}{3\mathcal{R}^2}, \quad (3.66)$$

where we have used Eq. (3.65). This situation is interpreted physically as the presence of a surface layer (or thin shell) at  $\Sigma$  having a distributional stress-energy tensor.

The corresponding surface stress-energy tensor  $\mathcal{S}^{AB}$  can be expressed in the perfect-fluid form [4, 121, 132]

$$\mathcal{S}^{AB} = (\sigma + \mathcal{P}) \mathcal{U}^A \mathcal{U}^B + \mathcal{P} h^{AB}, \quad (3.67)$$

where  $\sigma$  and  $\mathcal{P}$  denote the surface energy density and pressure, respectively, and  $\mathcal{U}^A$  the velocity of a static observer sitting at  $\Sigma$ . In our setup, it is not complicated to show that <sup>6</sup>

$$\sigma = 0, \quad (3.68)$$

$$\mathcal{P} = \frac{1}{16\pi} \left(1 - \frac{2M_\infty}{\mathcal{R}}\right)^{-1/2} \frac{c_{-1}r_d}{3\mathcal{R}^2}. \quad (3.69)$$

$\mathcal{S}^{AB}$  complies with the NEC, WEC, and SEC, and therefore does not call for exotic matter in the usual sense, while DEC is spoiled (since  $\sigma = 0$  and  $\mathcal{P} > 0$ ). However, the tangential pressure  $\mathcal{P} \sim c_{-1}r_d/\mathcal{R}^2$  and thus it can be arbitrarily small as  $c_{-1} \ll 1$  and  $r_d/\mathcal{R} \ll 1$ , which means that the resulting DEC violation is extremely mild. This situation is significantly better than in many thin-shell models where DEC and even weaker conditions fail (e.g., in Refs. [132–134] a thin layer with a negative surface energy density is considered), although DEC-satisfying constructions exist, like e.g. in Ref. [135].

Nevertheless, a different approach can also be pursued (this is related to so-called thick-shell or finite-width layers generalizations; see e.g. Refs. [136–140]). While a sharp junction at  $r = \mathcal{R}$  necessarily produces a surface layer, performing the matching across a narrow region  $r \in [\mathcal{R}, \mathcal{R} + \Delta]$ , with  $\Delta \ll \mathcal{R}$ , allows the metric to be smoothly interpolated between the logarithmic solution and the Schwarzschild exterior using an appropriately

---

<sup>6</sup>The dimension of  $\mathcal{P}$  is  $\sim 1/\mathcal{R}$  (or  $L^{-1}$ ), whereas from Eq. (2.32), the dimension of  $p_2$  is  $\sim 1/r^2$  (i.e.,  $L^{-2}$ ). This difference stems from the fact that  $\mathcal{P}$  is a surface pressure defined on a two-dimensional timelike hypersurface, while  $p_2$  is the usual bulk pressure defined in three-dimensional space.

chosen smooth function (e.g., a quintic polynomial). This construction can ensure continuity of both the metric and its first derivative, and hence can yield a fully regular matching procedure compatible with the classical energy conditions.

## 4 Concluding remarks

Classical energy conditions are essential to guarantee that Einstein field equations are sourced by “physically reasonable” matter and that the resulting solutions are physically admissible. In this work, we have examined their role in generic static, spherically symmetric spacetimes (2.1).

In models where  $-g_{tt} \neq g_{rr}^{-1}$  (see Sec. 2.1), the formation of an event horizon is often accompanied by NEC violations, and some classical expectations may break down. Such scenarios can lead to the emergence of effective impenetrable surfaces characterized by  $-g_{tt}g_{rr} \equiv AB = 0$ , where the stress-energy tensor typically exhibits a pathological behavior, with the energy density and pressures becoming divergent. Interestingly, this pattern is reminiscent of the firewall hypothesis [141], which proposes that infalling observers may encounter a high-energy surface and be destroyed upon reaching the black hole horizon.

Within the class of Kerr-Schild spacetimes (2.31) (see Sec. 2.2), we have developed a systematic procedure for deriving metrics obeying the NEC, where one simply selects the function  $y(r)$  fulfilling relation (2.33) and then solves the ensuing *ordinary* differential equation (2.34) for the component  $B(r)$ .

Among the several solutions that can be constructed via this algorithm, we have identified in Sec. 3 a particularly notable example that includes a logarithmic correction to the Schwarzschild model. Similar configurations have appeared in modified gravity patterns, but our Eq. (3.1) is distinctive in that it is framed within general relativity and satisfies *all* standard energy conditions. We have analyzed its parameter space by distinguishing between different classes of compact and ultra-compact objects according to the presence or absence of horizons and photon spheres, leading to the following operational classification (see Fig. 3 and Table 3): (i) “*bona fide*” black holes, characterized by the existence of at least one event horizon and a physical photon sphere; (ii) black hole mimickers, i.e., horizonless structures typically possessing both an unstable and a stable photon sphere and reproducing black-hole-like external observables; and (iii) more general “non-exotic compact objects”, which may or may not admit photon spheres and need not exhibit black-hole phenomenology. The log-metric can serve as an effective *geometric* candidate for the exterior spacetime of categories (i)-(iii), and, remarkably, it is not excluded by current EHT data. These results further strengthen the physical grounding of the aforementioned scheme for NEC-satisfying metrics, whose full potential remains to be explored. Being general and widely applicable, this method can potentially generate, beyond the specific case (3.1), a broad family of effective geometries able to describe new prototypes of compact bodies.

In the spirit of Ref. [90], the logarithmically corrected model may also be relevant for characterizing dark matter profiles that satisfy the standard energy conditions, although the underlying effective matter content is anisotropic, while cold dark matter is usually described as isotropic, pressureless dust [142]. On the other hand, we do not find any clear

indication that the log-geometry provides a viable dark energy paradigm. These points deserve a careful analysis in a separate paper.

## Acknowledgments

The work of Z. W. is supported by the National Natural Science Foundation of China (12405063). E. B. acknowledges the support of INFN *iniziativa specifica* Moonlight2.

## A Null energy condition in non-static and spherically symmetric geometries

Non-static and spherically symmetric metrics can be written as [126, 127]

$$ds^2 = -B(r, t)dt^2 + A(r, t)dr^2 + r^2d\Omega^2. \quad (\text{A.1})$$

In this geometry, the Ricci tensor  $R_{\mu\nu}$  generally loses its diagonal structure, and consequently the identification of an appropriate orthonormal frame that would diagonalize the energy-momentum tensor becomes significantly more involved. Nevertheless, for our purposes, we can simplify the analysis by restricting attention to radial geodesics. In this case, the radial four-velocity takes the form

$$\mathcal{V}^\mu = \left( \frac{\tilde{E}}{B(r, t)}, \mathcal{V}^r, 0, 0 \right), \quad (\text{A.2})$$

with

$$(\mathcal{V}^r)^2 = \frac{1}{A(r, t)} \left( \frac{\tilde{E}^2}{B(r, t)} - \alpha \right), \quad (\text{A.3})$$

and, like before,  $\alpha = 1$  for timelike geodesics and  $\alpha = 0$  for null ones. Here, we have defined

$$\tilde{E}(r, t) \equiv B(r, t) \frac{dt}{d\lambda}, \quad (\text{A.4})$$

which is no longer conserved along the geodesics, as  $\partial/\partial t$  is not a Killing vector.

The energy density measured by a radial timelike experimenter is given by

$$T_{\mu\nu}\mathcal{V}^\mu\mathcal{V}^\nu = \frac{1}{8\pi} \left( \frac{f_0}{r^2} + \frac{f_2\tilde{E}^2}{r^2} + \frac{f_3\tilde{E}}{r^2} \right), \quad (\text{A.5a})$$

where  $f_0(r, t)$  attains the same form as in Eq. (2.10) and

$$f_2(r, t) := -r \left( \frac{1}{AB} \right)', \quad (\text{A.5b})$$

$$f_3(r, t) := \frac{2r\dot{A}}{AB} \left( \frac{\tilde{E}^2/B - 1}{A} \right)^{1/2}, \quad (\text{A.5c})$$

the dot denoting partial differentiation with respect to  $t$ .

In analogy with the investigation in Sec. 2.1.1, Eq. (A.3) indicates that an infinite potential well may emerge where  $AB$  vanishes, provided  $\tilde{E} \neq 0$ . Furthermore, the energy density may diverge as the radially infalling observer approaches the location where  $AB = 0$ .

The NEC for a radial null vector requires that (cf. Eq. (1.1))

$$\frac{f_2 \tilde{E}^2}{r} + \frac{2\tilde{E}\dot{A} \left(\frac{\tilde{E}^2}{AB}\right)^{1/2}}{AB} \geq 0, \quad (\text{A.6})$$

which in the region where  $AB > 0$  and  $\tilde{E} > 0$  (recall that  $\tilde{E} > 0$  outside the event horizon of a black hole spacetime), boils down to

$$(\sqrt{AB})' \geq \dot{A}. \quad (\text{A.7})$$

For the specific case where  $A(r, t) = 1/B(r, t)$ , the NEC imposes the following constraint:

$$\frac{\tilde{E}|\tilde{E}|\dot{B}}{B^2} \leq 0, \quad (\text{A.8})$$

which in the domain where  $\tilde{E} > 0$  reduces to the requirement

$$\frac{\partial B(r, t)}{\partial t} \leq 0. \quad (\text{A.9})$$

## References

- [1] S.W. Hawking and G.F.R. Ellis, *The Large Scale Structure of Space-Time*, Cambridge Monographs on Mathematical Physics, Cambridge University Press (1973), [10.1017/9781009253161](https://doi.org/10.1017/9781009253161).
- [2] R.P. Geroch and G.T. Horowitz, *Global structure of spacetimes*, in *General Relativity: An Einstein Centenary Survey*, pp. 212–293 (1979).
- [3] M. Visser, *Lorentzian Wormholes. From Einstein to Hawking*, Springer, New York, USA (1995).
- [4] E. Poisson, *A Relativist's Toolkit: The Mathematics of Black-Hole Mechanics*, Cambridge University Press (12, 2009), [10.1017/CBO9780511606601](https://doi.org/10.1017/CBO9780511606601).
- [5] P. Martin-Moruno and M. Visser, *Classical and semi-classical energy conditions*, *Fundam. Theor. Phys.* **189** (2017) 193 [[1702.05915](https://arxiv.org/abs/1702.05915)].
- [6] E. Curiel, *A Primer on Energy Conditions*, *Einstein Stud.* **13** (2017) 43 [[1405.0403](https://arxiv.org/abs/1405.0403)].
- [7] E.-A. Kontou and K. Sanders, *Energy conditions in general relativity and quantum field theory*, *Class. Quant. Grav.* **37** (2020) 193001 [[2003.01815](https://arxiv.org/abs/2003.01815)].
- [8] P. Martin-Moruno and M. Visser, *Semiclassical energy conditions for quantum vacuum states*, *JHEP* **09** (2013) 050 [[1306.2076](https://arxiv.org/abs/1306.2076)].
- [9] C. Barcelo and M. Visser, *Scalar fields, energy conditions, and traversable wormholes*, *Class. Quant. Grav.* **17** (2000) 3843 [[gr-qc/0003025](https://arxiv.org/abs/gr-qc/0003025)].

- [10] J. Borissova, S. Liberati and M. Visser, *Timelike convergence condition in regular black-hole spacetimes with (anti-)de Sitter core*, *Phys. Rev. D* **112** (2025) 104072 [[2509.08590](#)].
- [11] R. Penrose, *Gravitational collapse and space-time singularities*, *Phys. Rev. Lett.* **14** (1965) 57.
- [12] S. Hawking, *The occurrence of singularities in cosmology. III. Causality and singularities*, *Proc. Roy. Soc. Lond. A* **300** (1967) 187.
- [13] S.W. Hawking and R. Penrose, *The Singularities of gravitational collapse and cosmology*, *Proc. Roy. Soc. Lond. A* **314** (1970) 529.
- [14] R. Schoen and S.-T. Yau, *Positivity of the total mass of a general space-time*, *Phys. Rev. Lett.* **43** (1979) 1457.
- [15] R. Schoen and S.-T. Yau, *On the Proof of the positive mass conjecture in general relativity*, *Commun. Math. Phys.* **65** (1979) 45.
- [16] G.T. Horowitz, *The positive energy theorem and its extensions*, in *Asymptotic Behavior of Mass and Spacetime Geometry*, F.J. Flaherty, ed., (Berlin, Heidelberg), pp. 1–21, Springer Berlin Heidelberg, 1984.
- [17] K.D. Olum, *Superluminal travel requires negative energies*, *Phys. Rev. Lett.* **81** (1998) 3567 [[gr-qc/9805003](#)].
- [18] M. Visser, B. Bassett and S. Liberati, *Superluminal censorship*, *Nucl. Phys. B Proc. Suppl.* **88** (2000) 267 [[gr-qc/9810026](#)].
- [19] R.M. Wald, *General Relativity*, Chicago Univ. Pr., Chicago, USA (1984), [10.7208/chicago/9780226870373.001.0001](#).
- [20] R.M. Wald, *The thermodynamics of black holes*, *Living Rev. Rel.* **4** (2001) 6 [[gr-qc/9912119](#)].
- [21] A.E. Mayo and J.D. Bekenstein, *No hair for spherical black holes: Charged and nonminimally coupled scalar field with selfinteraction*, *Phys. Rev. D* **54** (1996) 5059 [[gr-qc/9602057](#)].
- [22] C.A.R. Herdeiro and E. Radu, *Asymptotically flat black holes with scalar hair: a review*, *Int. J. Mod. Phys. D* **24** (2015) 1542014 [[1504.08209](#)].
- [23] L.H. Ford and T.A. Roman, *Averaged energy conditions and quantum inequalities*, *Phys. Rev. D* **51** (1995) 4277 [[gr-qc/9410043](#)].
- [24] C.J. Fewster, *Lectures on quantum energy inequalities*, [1208.5399](#).
- [25] F.S.N. Lobo, ed., *Wormholes, Warp Drives and Energy Conditions*, vol. 189 of *Fundamental Theories of Physics*, Springer (2017), [10.1007/978-3-319-55182-1](#), [[2103.05610](#)].
- [26] J.P.S. Lemos and O.B. Zaslavskii, *Black hole mimickers: Regular versus singular behavior*, *Phys. Rev. D* **78** (2008) 024040 [[0806.0845](#)].
- [27] R. Carballo-Rubio, F. Di Filippo, S. Liberati and M. Visser, *Phenomenological aspects of black holes beyond general relativity*, *Phys. Rev. D* **98** (2018) 124009 [[1809.08238](#)].
- [28] V. Cardoso and P. Pani, *Testing the nature of dark compact objects: a status report*, *Living Rev. Rel.* **22** (2019) 4 [[1904.05363](#)].
- [29] Y. Yang, D. Liu, A. Övgün, G. Lambiase and Z.-W. Long, *Rotating black hole mimicker surrounded by the string cloud*, *Phys. Rev. D* **109** (2024) 024002 [[2307.09344](#)].

- [30] R. Casadio, A. Kamenshchik and J. Ovalle, *From black hole mimickers to black holes*, *Phys. Rev. D* **109** (2024) 024042 [[2401.03980](#)].
- [31] C. Bambi et al., *Black hole mimickers: from theory to observation*, 5, 2025 [[2505.09014](#)].
- [32] M. De Laurentis and P. Pani, *Testing the nature of compact objects and the black hole paradigm*, *Gen. Rel. Grav.* **57** (2025) 39.
- [33] R. Carballo-Rubio et al., *Towards a non-singular paradigm of black hole physics*, *JCAP* **05** (2025) 003 [[2501.05505](#)].
- [34] R.-Z. Guo and Q.-G. Huang, *Gravitational Wave Tails and Transient Behaviors of Quantum-Corrected Black Holes*, [2601.00164](#).
- [35] S.D. Mathur, *The Fuzzball proposal for black holes: An Elementary review*, *Fortsch. Phys.* **53** (2005) 793 [[hep-th/0502050](#)].
- [36] K. Skenderis and M. Taylor, *The fuzzball proposal for black holes*, *Phys. Rept.* **467** (2008) 117 [[0804.0552](#)].
- [37] F. Rahaman, S. Chakraborty, S. Ray, A.A. Usmani and S. Islam, *The higher dimensional gravastars*, *International Journal of Theoretical Physics* **54** (2014) 50.
- [38] E. Mottola, *Gravitational Vacuum Condensate Stars*, [2302.09690](#).
- [39] D. Jampolski and L. Rezzolla, *On the formation of gravastars*, [2509.15302](#).
- [40] S.L. Liebling and C. Palenzuela, *Dynamical boson stars*, *Living Rev. Rel.* **26** (2023) 1 [[1202.5809](#)].
- [41] Y. Shmir, *Boson Stars*, *Lect. Notes Phys.* **1017** (2023) 347 [[2204.06374](#)].
- [42] M. Visser, *Traversable wormholes: Some simple examples*, *Phys. Rev. D* **39** (1989) 3182 [[0809.0907](#)].
- [43] M. Visser, S. Kar and N. Dadhich, *Traversable wormholes with arbitrarily small energy condition violations*, *Phys. Rev. Lett.* **90** (2003) 201102 [[gr-qc/0301003](#)].
- [44] S. Kar, N. Dadhich and M. Visser, *Quantifying energy condition violations in traversable wormholes*, *Pramana* **63** (2004) 859 [[gr-qc/0405103](#)].
- [45] E. Di Grezia, E. Battista, M. Manfredonia and G. Miele, *Spin, torsion and violation of null energy condition in traversable wormholes*, *Eur. Phys. J. Plus* **132** (2017) 537 [[1707.01508](#)].
- [46] M.R. Mehdizadeh and A.H. Ziaie, *Novel Casimir wormholes in Einstein gravity*, *Eur. Phys. J. Plus* **139** (2024) 1001 [[2406.03588](#)].
- [47] E. Battista, S. Capozziello and A. Errehymy, *Generalized uncertainty principle corrections in Rastall–Rainbow Casimir wormholes*, *Eur. Phys. J. C* **84** (2024) 1314 [[2409.09750](#)].
- [48] D. Horvat and S. Ilijic, *Gravastar energy conditions revisited*, *Class. Quant. Grav.* **24** (2007) 5637 [[0707.1636](#)].
- [49] P. Martin Moruno, N. Montelongo Garcia, F.S.N. Lobo and M. Visser, *Generic thin-shell gravastars*, *JCAP* **03** (2012) 034 [[1112.5253](#)].
- [50] A. Simpson and M. Visser, *Black-bounce to traversable wormhole*, *JCAP* **02** (2019) 042 [[1812.07114](#)].
- [51] F.S.N. Lobo, M.E. Rodrigues, M.V. de Sousa Silva, A. Simpson and M. Visser, *Novel*

- black-bounce spacetimes: wormholes, regularity, energy conditions, and causal structure*, *Phys. Rev. D* **103** (2021) 084052 [[2009.12057](#)].
- [52] C.W. Misner, K.S. Thorne and J.A. Wheeler, *Gravitation*, W. H. Freeman, San Francisco (1973).
- [53] M. Nakahara, *Geometry, topology and physics* (2003).
- [54] M.S. Morris and K.S. Thorne, *Wormholes in space-time and their use for interstellar travel: A tool for teaching general relativity*, *Am. J. Phys.* **56** (1988) 395.
- [55] L. Rezzolla and O. Zanotti, *Relativistic Hydrodynamics*, Oxford University Press (9, 2013), [10.1093/acprof:oso/9780198528906.001.0001](#).
- [56] I. Dymnikova, *Cosmological term as a source of mass*, *Class. Quant. Grav.* **19** (2002) 725 [[gr-qc/0112052](#)].
- [57] V. Faraoni, A. Giusti and T.F. Bean, *Asymptotic flatness and Hawking quasilocal mass*, *Phys. Rev. D* **103** (2021) 044026 [[2010.00069](#)].
- [58] M. Günther, *Skyrmion spacetime defect, degenerate metric, and negative gravitational mass*, Master's thesis, Karlsruhe Institute of Technology, September 2017.
- [59] G.T. Horowitz, *Topology change in classical and quantum gravity*, *Class. Quant. Grav.* **8** (1991) 587.
- [60] R.K. Kaul and S. Sengupta, *Degenerate spacetimes in first order gravity*, *Phys. Rev. D* **93** (2016) 084026 [[1602.04559](#)].
- [61] R. Kaul and S. Sengupta, *Degenerate extension of the Schwarzschild exterior*, *Phys. Rev. D* **96** (2017) 104011 [[1709.00188](#)].
- [62] F.R. Klinkhamer and Z.L. Wang, *Nonsingular bouncing cosmology from general relativity*, *Phys. Rev. D* **100** (2019) 083534 [[1904.09961](#)].
- [63] E. Battista, *Nonsingular bouncing cosmology in general relativity: physical analysis of the spacetime defect*, *Class. Quant. Grav.* **38** (2021) 195007 [[2011.09818](#)].
- [64] Z.L. Wang, *Regularized big bang singularity: Geodesic congruences*, *Phys. Rev. D* **104** (2021) 084093 [[2109.04229](#)].
- [65] S. Capozziello, S. De Bianchi and E. Battista, *Avoiding singularities in Lorentzian-Euclidean black holes: The role of atemporality*, *Phys. Rev. D* **109** (2024) 104060 [[2404.17267](#)].
- [66] A. Garnier and E. Battista, *Complex degenerate metrics in general relativity: a covariant extension of the Moore–Penrose algorithm*, *Eur. Phys. J. C* **85** (2025) 284 [[2502.10053](#)].
- [67] S. Capozziello, E. Battista and S. De Bianchi, *Null geodesics, causal structure, and matter accretion in Lorentzian-Euclidean black holes*, *Phys. Rev. D* **112** (2025) 044009 [[2507.08431](#)].
- [68] S. De Bianchi, S. Capozziello and E. Battista, *Atemporality from Conservation Laws of Physics in Lorentzian-Euclidean Black Holes*, *Found. Phys.* **55** (2025) 36 [[2504.17570](#)].
- [69] E. Battista, S. Capozziello and C.-Y. Chen, *Shadow signatures and energy accumulation in Lorentzian-Euclidean black holes*, [2601.10806](#).
- [70] Z.-L. Wang, *Geodesic congruences in modified Schwarzschild black holes*, *Eur. Phys. J. C* **82** (2022) 901.

- [71] P.S. Joshi, D. Malafarina and R. Narayan, *Equilibrium configurations from gravitational collapse*, *Class. Quant. Grav.* **28** (2011) 235018 [[1106.5438](#)].
- [72] P.S. Joshi, D. Malafarina and R. Narayan, *Distinguishing black holes from naked singularities through their accretion disc properties*, *Class. Quant. Grav.* **31** (2014) 015002 [[1304.7331](#)].
- [73] R. Shaikh, P. Kocherlakota, R. Narayan and P.S. Joshi, *Shadows of spherically symmetric black holes and naked singularities*, *Mon. Not. Roy. Astron. Soc.* **482** (2019) 52 [[1802.08060](#)].
- [74] P. Hassan Puttasiddappa, D.C. Rodrigues and D.F. Mota, *Shadows of naked singularity in Brans-Dicke gravity*, **2505.23204**.
- [75] N.V.D. Bergh, *General solutions for a static isotropic metric in the Brans-Dicke gravitational theory*, *Gen. Rel. Grav.* **12** (1980) 863.
- [76] M. Del Piano, S. Hohenegger and F. Sannino, *Quantum black hole physics from the event horizon*, *Phys. Rev. D* **109** (2024) 024045 [[2307.13489](#)].
- [77] E. Battista, *Quantum Schwarzschild geometry in effective field theory models of gravity*, *Phys. Rev. D* **109** (2024) 026004 [[2312.00450](#)].
- [78] Z.-L. Wang and E. Battista, *Dynamical features and shadows of quantum Schwarzschild black hole in effective field theories of gravity*, *Eur. Phys. J. C* **85** (2025) 304 [[2501.14516](#)].
- [79] Z.-L. Wei, J. Zhang, Y. Xie and P.-L. Yin, *Probing a one-loop quantum-corrected Schwarzschild spacetime with precessing and periodic motion*, *Eur. Phys. J. C* **85** (2025) 698.
- [80] S. Hohenegger, *Probing Effective Black Hole Deformations*, **2508.17781**.
- [81] G. Chapline, E. Hohlfeld, R.B. Laughlin and D.I. Santiago, *Quantum phase transitions and the breakdown of classical general relativity*, *Int. J. Mod. Phys. A* **18** (2003) 3587 [[gr-qc/0012094](#)].
- [82] T. Jacobson, *When is  $g(tt)g(rr) = -1$ ?*, *Class. Quant. Grav.* **24** (2007) 5717 [[0707.3222](#)].
- [83] J. Ovalle, *Black holes without Cauchy horizons and integrable singularities*, *Phys. Rev. D* **107** (2023) 104005 [[2305.00030](#)].
- [84] I. Dymnikova, *Spherically symmetric space-time with the regular de Sitter center*, *Int. J. Mod. Phys. D* **12** (2003) 1015 [[gr-qc/0304110](#)].
- [85] A. Bonanno and M. Reuter, *Renormalization group improved black hole space-times*, *Phys. Rev. D* **62** (2000) 043008 [[hep-th/0002196](#)].
- [86] S.A. Hayward, *Formation and evaporation of regular black holes*, *Phys. Rev. Lett.* **96** (2006) 031103 [[gr-qc/0506126](#)].
- [87] P. Bargueño, S. Bravo Medina, M. Nowakowski and D. Batic, *Quantum Mechanical Corrections to the Schwarzschild Black Hole Metric*, *EPL* **117** (2017) 60006 [[1605.06463](#)].
- [88] J. Lewandowski, Y. Ma, J. Yang and C. Zhang, *Quantum Oppenheimer-Snyder and Swiss Cheese Models*, *Phys. Rev. Lett.* **130** (2023) 101501 [[2210.02253](#)].
- [89] F. Ahmed, A. Al-Badawi and M. Fathi, *Some phenomenological aspects of a quantum-corrected Reissner-Nordström black hole: quasi-periodic oscillations, scalar perturbations and thermal fluctuations*, **2602.15551**.

- [90] M.-H. Li and K.-C. Yang, *Galactic Dark Matter in the Phantom Field*, *Phys. Rev. D* **86** (2012) 123015 [[1204.3178](#)].
- [91] J.A. Méndez-Zavaleta, E. Rojas and J.J. Suárez-Garibay, *Classical emergence of the quantum-backreacted BTZ black hole from exponential electrodynamics*, [2601.18967](#).
- [92] S.E.P. Bergliaffa, R. Maier and N.d.O. Silvano, *Hairy Black Holes from Horndeski Theory*, [2107.07839](#).
- [93] F. D’Ambrosio, S.D.B. Fell, L. Heisenberg and S. Kuhn, *Black holes in  $f(Q)$  gravity*, *Phys. Rev. D* **105** (2022) 024042 [[2109.03174](#)].
- [94] L. Blanchet, *Post-Newtonian Theory for Gravitational Waves*, *Living Rev. Rel.* **17** (2014) 2 [[1310.1528](#)].
- [95] P.T. Chrusciel, M.A.H. MacCallum and D.B. Singleton, *Gravitational waves in general relativity: 14. Bondi expansions and the polyhomogeneity of Scri*, [gr-qc/9305021](#).
- [96] X. He, X. Wu and N. Xie, *Bondi mass, memory effect and balance law of polyhomogeneous spacetime*, *Class. Quant. Grav.* **43** (2026) 015022 [[2504.07774](#)].
- [97] R.M. Corless, G.H. Gonnet, D.E.G. Hare, D.J. Jeffrey and D.E. Knuth, *On the lambert W function*, *Advances in Computational Mathematics* **5** (1996) 329.
- [98] *Nist digital library of mathematical functions*, <https://dlmf.nist.gov> .
- [99] G.J. Olmo, J.L. Rosa, D. Rubiera-Garcia and D. Saez-Chillon Gomez, *Shadows and photon rings of regular black holes and geonic horizonless compact objects*, *Class. Quant. Grav.* **40** (2023) 174002 [[2302.12064](#)].
- [100] R. Narayan, M.D. Johnson and C.F. Gammie, *The Shadow of a Spherically Accreting Black Hole*, *Astrophys. J. Lett.* **885** (2019) L33 [[1910.02957](#)].
- [101] V. Perlick and O.Y. Tsupko, *Calculating black hole shadows: Review of analytical studies*, *Phys. Rept.* **947** (2022) 1 [[2105.07101](#)].
- [102] M. Afrin, S. Vagnozzi and S.G. Ghosh, *Tests of Loop Quantum Gravity from the Event Horizon Telescope Results of Sgr A\**, *Astrophys. J.* **944** (2023) 149 [[2209.12584](#)].
- [103] S. Vagnozzi et al., *Horizon-scale tests of gravity theories and fundamental physics from the Event Horizon Telescope image of Sagittarius A*, *Class. Quant. Grav.* **40** (2023) 165007 [[2205.07787](#)].
- [104] V. Vertogradov and A. Övgün, *General approach on shadow radius and photon spheres in asymptotically flat spacetimes and the impact of mass-dependent variations*, *Phys. Lett. B* **854** (2024) 138758 [[2404.18536](#)].
- [105] Z.-L. Wang, *Exploring the role of accretion disk geometry in shaping black hole shadows*, *Phys. Rev. D* **112** (2025) 064052 [[2506.21148](#)].
- [106] Y.-Y. Wu, Z.-L. Wang and Y.-Z. Li, *On the geodesics and shadows of Schwarzschild black holes with topological corrections*, *Int. J. Geom. Meth. Mod. Phys.* **23** (2026) 2550155.
- [107] S. Vagnozzi et al., *Horizon-scale tests of gravity theories and fundamental physics from the Event Horizon Telescope image of Sagittarius A*, *Class. Quant. Grav.* **40** (2023) 165007 [[2205.07787](#)].
- [108] Z.-L. Wang, *Shadows and rings of a de Sitter–Schwarzschild black hole*, *Eur. Phys. J. Plus* **138** (2023) 1131 [[2307.12361](#)].

- [109] X.-J. Gao, T.-T. Sui, X.-X. Zeng, Y.-S. An and Y.-P. Hu, *Investigating shadow images and rings of the charged Horndeski black hole illuminated by various thin accretions*, *Eur. Phys. J. C* **83** (2023) 1052 [2311.11780].
- [110] J.-W. Li, Z.-L. Wang and T.-T. Sui, *Shadows of quintessence black holes: spherical accretion, photon trajectories, and geodesic observers*, *Eur. Phys. J. C* **86** (2026) 335 [2603.09159].
- [111] EVENT HORIZON TELESCOPE collaboration, *First Sagittarius A\* Event Horizon Telescope Results. VI. Testing the Black Hole Metric*, *Astrophys. J. Lett.* **930** (2022) L17 [2311.09484].
- [112] K. Salahshoor and K. Nozari, *Circular orbits and accretion process in a class of Horndeski/Galileon black holes*, *Eur. Phys. J. C* **78** (2018) 486 [1806.08949].
- [113] G. Mustafa, F. Javed, A. Ditta, S.K. Maurya, Y. Liu and F. Atamurotov, *Matter accretion onto charged black holes in symmergent gravity*, *Physics of the Dark Universe* **42** (2023) 101376.
- [114] I.V. Chilingarian, I.Y. Katkov, I.Y. Zolotukhin, K.A. Grishin, Y. Beletsky, K. Boutsia et al., *A Population of Bona Fide Intermediate Mass Black Holes Identified as Low Luminosity Active Galactic Nuclei*, *Astrophys. J.* **863** (2018) 1 [1805.01467].
- [115] P.V.P. Cunha, E. Berti and C.A.R. Herdeiro, *Light-Ring Stability for Ultracompact Objects*, *Phys. Rev. Lett.* **119** (2017) 251102 [1708.04211].
- [116] G.J. Olmo, D. Rubiera-Garcia and D.S.-C. Gómez, *New light rings from multiple critical curves as observational signatures of black hole mimickers*, *Phys. Lett. B* **829** (2022) 137045 [2110.10002].
- [117] G. Guo, Y. Lu, P. Wang, H. Wu and H. Yang, *Black holes with multiple photon spheres*, *Phys. Rev. D* **107** (2023) 124037 [2212.12901].
- [118] Z.-L. Wang and E. Battista, *Energy conditions and families of regular spacetimes*, *In preparation* (2026) .
- [119] S. Rosswog, *SPH Methods in the Modelling of Compact Objects*, *Liv. Rev. Comput. Astrophys.* **1** (2015) 1 [1406.4224].
- [120] M.S.R. Delgaty and K. Lake, *Physical acceptability of isolated, static, spherically symmetric, perfect fluid solutions of Einstein's equations*, *Comput. Phys. Commun.* **115** (1998) 395 [gr-qc/9809013].
- [121] M. Visser and D.L. Wiltshire, *Stable gravastars: An Alternative to black holes?*, *Class. Quant. Grav.* **21** (2004) 1135 [gr-qc/0310107].
- [122] C.A.R. Herdeiro, *Black Holes: On the Universality of the Kerr Hypothesis*, *Lect. Notes Phys.* **1017** (2023) 315 [2204.05640].
- [123] M. Bezares and N. Sanchis-Gual, *Exotic Compact Objects: A Recent Numerical-Relativity Perspective*, (2025), DOI [2406.04901].
- [124] R. Carballo-Rubio, F. Di Filippo, S. Liberati, C. Pacilio and M. Visser, *Inner horizon instability and the unstable cores of regular black holes*, *JHEP* **05** (2021) 132 [2101.05006].
- [125] C.M. Will, *The Confrontation between General Relativity and Experiment*, *Living Rev. Rel.* **17** (2014) 4 [1403.7377].

- [126] S. Weinberg, *Gravitation and Cosmology: Principles and Applications of the General Theory of Relativity*, John Wiley and Sons, New York (1972).
- [127] S.M. Carroll, *Spacetime and Geometry: An Introduction to General Relativity*, Cambridge University Press (7, 2019), [10.1017/9781108770385](https://doi.org/10.1017/9781108770385).
- [128] C.M. Will, *Theory and experiment in gravitational physics*, Cambridge university press (2018).
- [129] T. Clifton and J.D. Barrow, *The Power of General Relativity*, *Phys. Rev. D* **72** (2005) 103005 [[gr-qc/0509059](https://arxiv.org/abs/gr-qc/0509059)].
- [130] I.I. Shapiro, C.C. Counselman III and R.W. King, *Verification of the principle of equivalence for massive bodies*, *Physical Review Letters* **36** (1976) 555.
- [131] GRAVITY collaboration, *Detection of the Schwarzschild precession in the orbit of the star S2 near the Galactic centre massive black hole*, *Astron. Astrophys.* **636** (2020) L5 [[2004.07187](https://arxiv.org/abs/2004.07187)].
- [132] T. Berry, F.S.N. Lobo, A. Simpson and M. Visser, *Thin-shell traversable wormhole crafted from a regular black hole with asymptotically Minkowski core*, *Phys. Rev. D* **102** (2020) 064054 [[2008.07046](https://arxiv.org/abs/2008.07046)].
- [133] E. Poisson and M. Visser, *Thin shell wormholes: Linearization stability*, *Phys. Rev. D* **52** (1995) 7318 [[gr-qc/9506083](https://arxiv.org/abs/gr-qc/9506083)].
- [134] M. Sharif and S. Mumtaz, *Schwarzschild-de Sitter and Anti-de Sitter Thin-Shell Wormholes and Their Stability*, *Adv. High Energy Phys.* **2014** (2014) 639759.
- [135] P.R. Brady, J. Louko and E. Poisson, *Stability of a shell around a black hole*, *Phys. Rev. D* **44** (1991) 1891.
- [136] C. Cattoen, T. Faber and M. Visser, *Gravastars must have anisotropic pressures*, *Class. Quant. Grav.* **22** (2005) 4189 [[gr-qc/0505137](https://arxiv.org/abs/gr-qc/0505137)].
- [137] T. Berry, A. Simpson and M. Visser, *General-relativistic thin-shell Dyson megaspheres*, *Phys. Rev. D* **106** (2022) 084001 [[2207.02465](https://arxiv.org/abs/2207.02465)].
- [138] D. Jampolski and L. Rezzolla, *Nested solutions of gravitational condensate stars*, *Class. Quant. Grav.* **41** (2024) 065014 [[2310.13946](https://arxiv.org/abs/2310.13946)].
- [139] F. Di Filippo and L. Rezzolla, *Can light-rings self-gravitate?*, *Phys. Rev. D* **111** (2025) L021504 [[2407.13832](https://arxiv.org/abs/2407.13832)].
- [140] F. Rahaman, B.S. Choudhury, A. Sanyal, A. Islam and B. Samanta, *Exact gravastar solution*, *Phys. Lett. B* **876** (2026) 140412 [[2604.09719](https://arxiv.org/abs/2604.09719)].
- [141] A. Almheiri, D. Marolf, J. Polchinski and J. Sully, *Black Holes: Complementarity or Firewalls?*, *JHEP* **02** (2013) 062 [[1207.3123](https://arxiv.org/abs/1207.3123)].
- [142] V. Mukhanov, *Physical Foundations of Cosmology*, Cambridge University Press, Oxford (2005), [10.1017/CBO9780511790553](https://doi.org/10.1017/CBO9780511790553).